Femtosecond laser written photonic and microfluidic circuits in diamond

IOP Publishing Journal Title
Journal **XX** (XXXX) XXXXXX https://doi.org/XXXX/XXXX

Femtosecond laser written photonic and microfluidic circuits in diamond

Vibhav Bharadwaj[1,2], Ottavia Jedrkiewicz[3], J. P. Hadden[4,5], Belén Sotillo[1,6], María Ramos Vázquez[7,8], Paola Dentella[2], Toney T. Fernandez[1], Andrea Chiappini[9], Argyro N. Giakoumaki[1,2], Thien Le Phu[1,2], Monica Bollani[3], Maurizio Ferrari[9], Roberta Ramponi[1,2], Paul E. Barclay[4] and Shane M. Eaton[1,2]

[1] Institute for Photonics and Nanotechnologies (IFN) - CNR, Milano, Italy
[2] Department of Physics, Politecnico di Milano, Milano, Italy
[3] Institute for Photonics and Nanotechnologies (IFN) - CNR, Como, Italy
[4] Institute for Quantum Science and Technology, University of Calgary, Calgary, Canada
[5] School of Physics and Astronomy, Cardiff University, Cardiff, UK
[6] Department of Materials Physics, Complutense University of Madrid, Madrid, Spain
[7] Centre for Disruptive Photonic Technologies, Nanyang Technological University, Singapore
[8] ICRM, Interdisciplinary Graduate School, Nanyang Technological University, Singapore
[9] Institute for Photonics and Nanotechnologies (IFN) - CNR, CSMFO and FBK-CMM, Trento, Italy

E-mail: vibhavbharadwaj@gmail.com

Received xxxxxx
Accepted for publication xxxxxx
Published xxxxxx

Abstract

Diamond has attracted great interest in the quantum optics community thanks to its nitrogen vacancy (NV) center, a naturally occurring impurity that is responsible for the pink coloration of some diamond crystals. The NV spin state with the brighter luminescence yield can be exploited for spin readout, exhibiting millisecond spin coherence times at ambient temperature. In addition, the energy levels of the ground state triplet of the NV are sensitive to external fields. These properties make NVs attractive as a scalable platform for efficient nanoscale resolution sensing based on electron spins and for quantum information systems. Integrated diamond photonics would be beneficial for optical magnetometry, due to the enhanced light-matter interaction and associated collection efficiency provided by waveguides, and for quantum information, by means of the optical linking of NV centers for long-range entanglement. Diamond is also compelling for microfluidic applications due to its outstanding biocompatibility, with sensing functionality provided by NV centers. Furthermore, laser written micrographitic modifications could lead to efficient and compact detectors of high energy radiation in diamond. However, it remains a challenge to fabricate optical waveguides, graphitic lines, NVs and microfluidics in diamond. In this Review, we describe a disruptive laser nanofabrication method based on femtosecond laser writing to realize a 3D micro-nano device toolkit for diamond. Femtosecond laser writing is advantageous compared to other state of the art fabrication technologies due to its versatility in forming diverse micro and nanocomponents in diamond. We describe how high quality buried optical waveguides, low roughness microfluidic channels, and on-demand NVs with excellent spectral properties can be laser formed in single-crystal diamond. We show the first integrated quantum photonic circuit in diamond consisting of an optically addressed NV for quantum information studies. The rapid progress of the field is encouraging but there are several challenges which must be met to realize future quantum technologies in diamond. We elucidate how these hurdles can be overcome using femtosecond laser fabrication, to realize both quantum computing and nanoscale magnetic field sensing devices in synthetic diamond.

IOP Publishing Journal Title
Journal **XX** (XXXX) XXXXXX https://doi.org/XXXX/XXXX

Keywords: Ultrafast laser writing, diamond, sensing, quantum optics, quantum computing, femtosecond laser

1. Background

1.1 Nitrogen vacancy centers in diamond

Diamond has generated significant interest in the scientific community, not only due its perfection in terms of its hardness and transparency but also due to a naturally occurring imperfection called the nitrogen vacancy (NV) color center defect. The NV center is formed when two of the carbons in the tetrahedral lattice structure of diamond is replaced by a nitrogen and a vacancy adjacent to it, as shown in Fig. 1(a). In its negatively charged state (NV^-, referred to as NV for simplicity in the subsequent text), the electronic ground state forms a spin triplet which can be polarized by excitation with 532 nm wavelength light. The resulting relaxation leads to a photoluminescence emission with a zero-phonon line (ZPL) at 637 nm. However, one of the spin states fluoresces more brightly than the other, due to the presence of an alternative non-radiative decay path when excited from the other state, as shown in Fig. 1(b). This spin dependent fluorescence emission can be utilized for optical readout of the spin state [1].

Diamond's largely spinless carbon lattice, along with the NV center's weak spin-orbit coupling makes it an ideal low noise solid-state spin system, with exceptional room temperature spin coherence of up to ~1 ms, comparable to trapped ions [2]. Additionally, since the spin states are sensitive to magnetic [3] and electric fields [4] through the Zeeman and Stark effects, respectively and NV centers in diamond have been shown to operate as atomic sized magnetometers with exceptional spatial resolutions and sensitivities comparable with the existing technologies, as depicted in Fig.1(c). Depending on the properties of the host diamond and its processing, NV centers can appear both as single isolated defects, and in high density ensembles. These properties make diamond NVs very attractive as a compact and scalable platform for quantum information processing systems and for high sensitivity electromagnetic field quantum sensors [5,6].

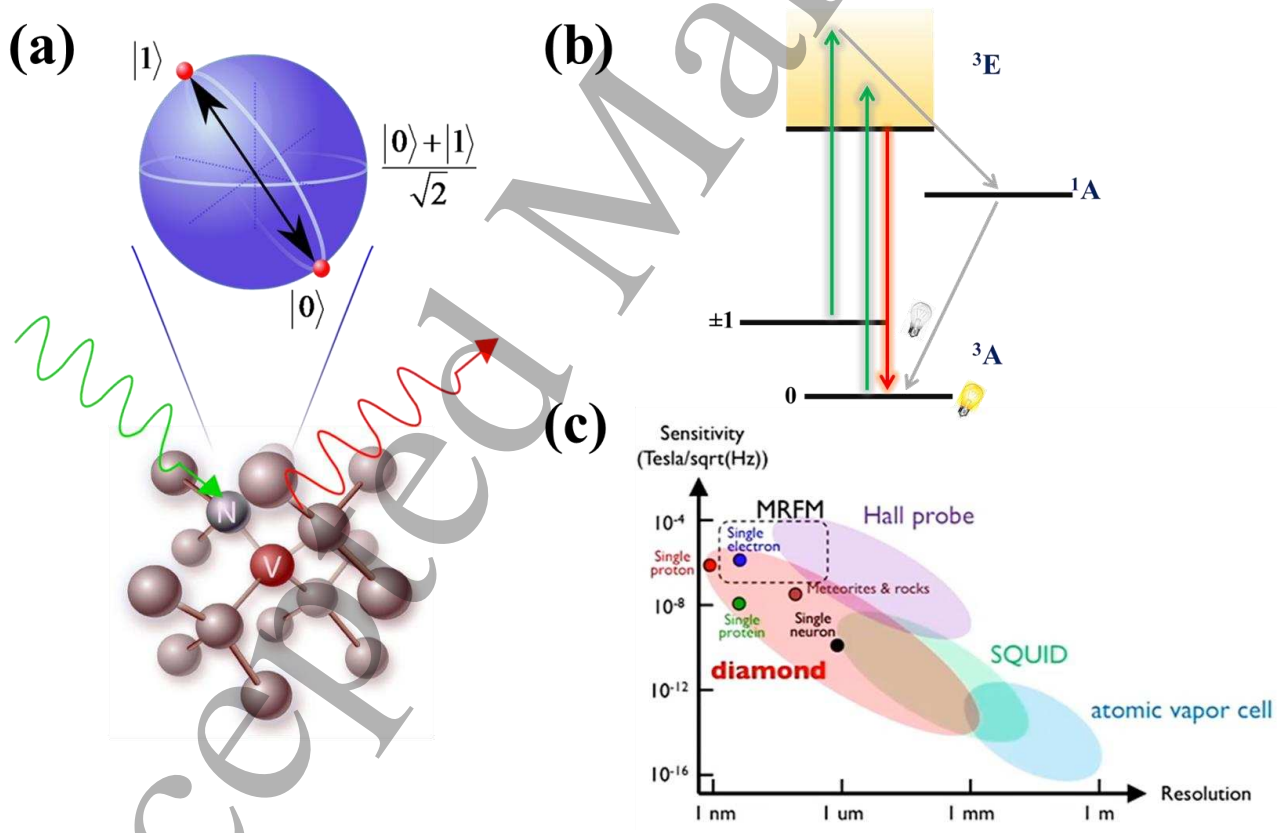

Fig. 1: (a) Schematic showing the crystal structure of diamond with NV center which can be exploited as a qubit. (b) Electronic energy level diagram of the ground state of NV center showing the alternative non-radiative decay path when excited from the ground states $m_s = \pm 1$. (c) Schematic chart depicting today's competitive magnetometric techniques based on their sensitivity and resolution [7].

1.2 Photolithographic diamond waveguide fabrication and its limitations

Optical waveguide fabrication in single crystal diamond has been a highly challenging task due to its hardness, high refractive index and low electrical conductivity. Nevertheless, waveguiding structures have been fabricated by engineering high refractive index material on diamond substrates [8,9], but leading to weak coupling with NVs near the surface. The first optical waveguide within a single crystal diamond was fabricated using the focused ion beam (FIB) technique by P. Olivero *et al.* [10] in 2005, shown in Fig. 2(a). However, the fabrication method led to undesirable stress in the diamond films leading to poor NV spectral properties [11]. Also, the waveguide length was limited to a few hundreds of micrometers due to the limitation of scaling the FIB fabrication process.

Waveguide fabrication within diamond has been demonstrated, primarily by selective etching of diamond to form an air-diamond interface. M.P Hiscocks *et al.* [12] succeeded in creating few millimeter-long waveguides using a scalable photolithography and reactive ion etching (RIE) technique. Typically, these etching methods are cumbersome and multi-step processes, involving ion implantation, high temperature annealing, etching of the waveguides into the diamond using RIE, and FIB to make 45° cuts into the waveguides to act as total internal reflection mirrors. Further improvement on the etching process was realized using suspended triangular nanobeam waveguides with an angled plasma etching process [13], as depicted in Fig. 2(b). The losses were about 10 dB/cm at visible wavelengths and a custom Faraday cage was required for each specific design.

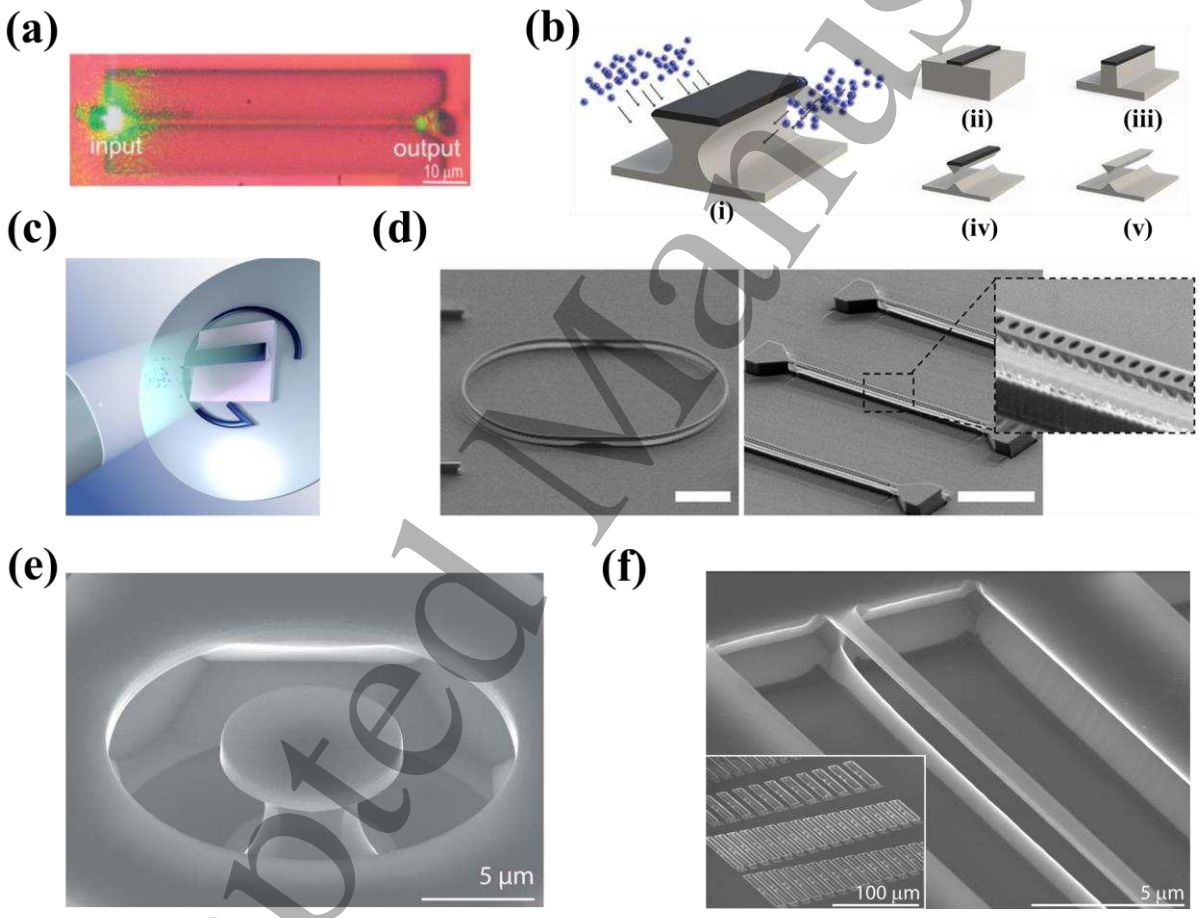

Fig. 2: (a) Microscope image showing light input and output from waveguide formed by FIB on diamond [10]. (b) Schematic showing steps involved in angled-etching to realize free-standing structures in bulk single-crystal diamond. (i) illustration of angle etching which involves: (ii) formation of the etch mask on the substrate, (iii) transferring the etch pattern into the substrate by conventional top down plasma etching, (iv) angled-etching to realize suspended nanobeam structures and finally, (v) removal of the residual etch mask [13]. (c) Graphical depiction of reactive ion beam angled etching showing the ion beam and the sample holder which can be rotated and tilted allowing uniform etching [14]. (d) Scanning electron microscope (SEM) images of a fabricated diamond racetrack resonator supported from the bottom and diamond nanobeam photonic crystal cavity operating at visible wavelengths. Scale bars are 10 μm and 5 μm respectively [13]. (e) Micro-disk and (f) nano-beam waveguide fabricated on single-crystal diamond using undercut etching technique [15,16].

Free-standing triangular structures have been fabricated on diamond using a novel reactive ion beam angled etching using a rotating and tilting sample stage allowing uniform etching, without the use of a Faraday cage, as depicted in Fig. 2(c) [14]. Angle etching techniques have been used to fabricate race-track resonators and nanobeam structures, as shown in Fig. 2(d). Further developments in preserving vertical etching during RIE has been performed by employing undercut etching procedures involving a plasma to quasi-isotropically etch along the planes of the diamond crystals and the desired structures being undercut [15,16]. High *Q/V* microdisks and nano-beam waveguides have been fabricated using the undercut etching technique, as shown in Fig. 2 (e), (f). Other techniques like direct ion microbeam writing has been used to create shallow multimode waveguides but the method is restricted to 2D waveguide geometries [17]. Recently, focused proton beam has been used to form single mode waveguides in the bulk of diamond offering a promising fabrication technique for bulk waveguide creation [18].

The above-mentioned techniques have led to numerous diamond NV-based applications in the recent past, but they are unable to form 3D waveguides within the bulk of diamond, where the NV coherence times are greatly improved [19]. In addition, these methods are limited to two-dimensional waveguiding structures and are complex multi-step techniques involving extensive material processing, clean room facilities and multi-million euro laboratories. More importantly, most of the waveguiding structures are not easily compatible with existing fiber-optic technologies. A new fabrication approach which addresses these issues would benefit the development of high-performance NV-based quantum technologies.

1.3 Femtosecond laser micromachining – A unique tool for optical photonic network inscription

Femtosecond laser micromachining has emerged as a very powerful tool for inscribing optical photonic networks in transparent dielectrics and crystals, beginning with its first demonstration in 1996 by Hirao's group [20]. The versatile microfabrication technique uses tightly focused ultrashort laser pulses inside a transparent material to selectively deposit energy within the focal due to nonlinear absorption (multiphoton and tunnelling) and avalanche ionization [21–23].

Depending on the absorbed energy at the focal point, different regimes of material modification can occur. In glasses, if the absorbed energy is too high, material damage occurs at the focal volume, leading to the formation of void-like structures [24]; for lower pulse energy, there is a regime in which the material undergoes a permanent refractive index change. This occurs due to contributions from various mechanisms such as color center formation [25], thermal heating followed by cooling leading to re-solidification [26,27], modification of chemical bonds in the material matrix creating an increase in density [28]. In multicomponent glasses, ion migration plays a crucial role in the resulting refractive index distribution [29–31]. By translating the sample and hence the laser focus inside the glass substrate, advanced optical photonic circuits can be formed, including those with three dimensional layouts [32–34].

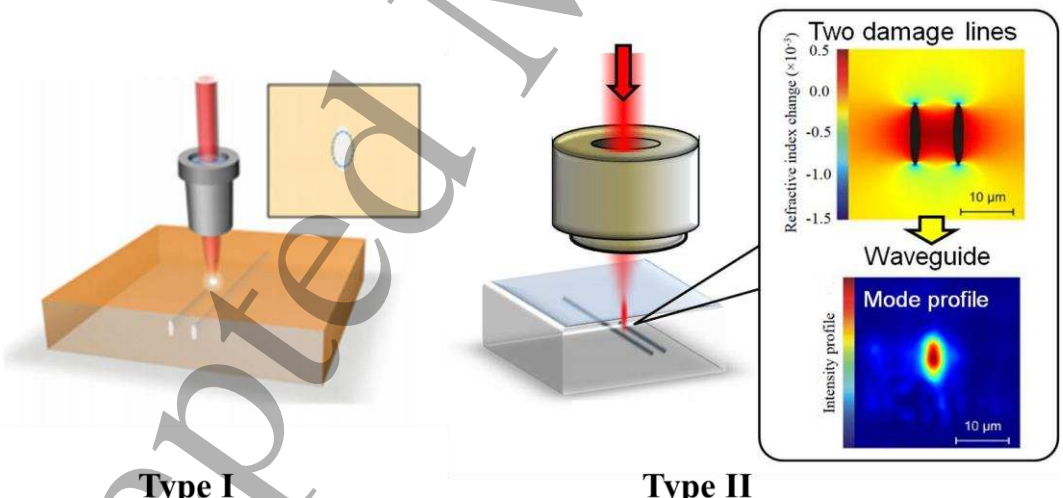

Fig. 3: Schematic showing the two modalities of femtosecond laser writing of waveguides. Type I modality: a single line of increased refractive index modification acting as the core for the optical waveguiding is laser formed. This is generally employed for laser writing in glasses [35]. Type II modality: two lines of decreased refractive index are laser written close to each other, creating a stressed central region between them and confining the optical mode between the two lines. The type II modality is generally employed for laser writing of optical waveguides in crystals.

In crystals, femtosecond laser irradiation generally produces a decrease in refractive index at the focal volume. This is due to the creation of lattice disorder at the focal volume leading to a lower density. Despite the negative refractive index change, optical waveguiding may occur on the sides of the modified region, where stresses induce a refractive index increase [36,37]. One of the most common ways of creating an optical waveguide in a crystal is by writing two closely spaced modification lines, resulting in a stressed central region in between, thus providing optical confinement. This geometry of laser writing is commonly referred to as a Type II modification, as depicted in Fig. 3. By tailoring the geometry of the modification, photonic structures have been realized in crystals such as lithium niobate ($LiNbO_3$) [38], silicon [39], potassium gadolinium tungstate (KGW) [40], yttrium aluminium garnet (YAG) [41], zinc selenide (ZnSe) [42], potassium titanium oxide phosphate (KTP) [43] and yttrium orthosilicate doped with praseodymium ($Pr:Y_2SiO_5$) [44].

The main advantages of femtosecond laser inscription compared to photolithography and other conventional microfabrication techniques are:

- Simple and low-cost setup. In femtosecond laser writing, there is no need for extensive sample preparation, masks or clean-room facilities.
- 3D structuring. Since the material modification occurs only at the focal volume due to nonlinear absorption, microstructures may be formed along 3D paths by translating the sample with respect to the laser focus using computer-controlled motion stages. Alternatively, one can keep the sample stationary and translate the laser focus using galvo scanners.
- Rapid prototyping. Femtosecond laser fabrication is a direct writing method requiring no mask. By simply changing the algorithm of the computer-controlled translation stages, one can realize arbitrary 3D optical circuits.
- Versatility. Femtosecond laser writing has been successfully applied to hundreds of different transparent materials including active [45] and passive [46] glasses, nonlinear glasses [47,48], ceramics [49], crystals [35] and polymers [50].
- Different modalities of microfabrication. Femtosecond laser writing can be applied in different modalities including: (1) bulk optical waveguide writing [20]; (2) bulk modification followed by chemical etching to produce hollow and buried microchannels [51]; (3) surface laser ablation by scanning the focus along the sample surface to form microfluidic channels, microholes and diffractive optics [52]; (4) two-photon polymerization to form 3D microstructures in photoresists [53–56].

These compelling advantages of the femtosecond laser writing have motivated major scientific research projects by groups all over the world. Twenty years since the original paper by Davis *et al.*, there are over 2500 citations to the original work, with demonstrations of devices including directional couplers [57], Y-splitters [58], polarization controllers [59], Bragg reflectors [60], interferometers [61], waveguide lasers [62], for novel applications in fields such as astrophotonics [63], quantum information [64], telecommunications [65], sensing [66], lab on a chip [67] and lab on a fiber [68].

In addition, industry is actively pursuing femtosecond laser microfabrication to meet the needs of modern and future technologies. Laser companies such as Spectra Physics, Coherent, Light conversion, IMRA America and Menlo systems are now producing high-repetition rate/energy femtosecond lasers tailored for femtosecond laser microfabrication. In addition, a laser processing technology developed by Nanoscribe (Eggenstein-Leopoldshafen, Germany), provides user-friendly and fully integrated femtosecond laser fabrication systems for 3D direct laser writing in photoresists. Most importantly, start-up companies have begun exploiting femtosecond laser writing to fabricate real world devices for end users. For example, Optoscribe (Livingston, Scotland), laser forms 3D waveguides and photonic lanterns for optical communications and astrophotonics; OZ optics (Ottawa, Canada) produces customized optical power taps, FemtoFiberTec (Berlin, Germany) fabricates fiber Bragg gratings for temperature, strain, pressure, and vibration measurement; FEMTOprint (Muzzano, Switzerland) realizes microphotonics in glass and polymers for micromechanics/optomechanics, and 5D high density memories; Incise Photonics (Toronto, Canada) write waveguide and microchannel devices directly in fibers for integrated lab-on-a-fiber devices; Modular photonics (Sydney, Australia) specializes in micro-chip fabrication in glass for applications in passive multiplexer devices for fiber networking.

1.4 CVD diamond properties

Single crystal diamond is preferred for laser writing, since waveguides in polycrystalline diamond would be lossy due to absorption and scattering at the boundaries. Moreover, single crystal diamond provides a more uniform environment for NV related applications. Chemical vapour deposition (CVD) has emerged as a suitable diamond growth technique to form diamond substrates for applications in spintronics due to its ability to precisely control impurity levels and tailor the electronic and optical properties of the diamond [69]. The well-known properties of its extremely high strength (Vickers hardness of about 10000 kg/mm^2) and high refractive index (about 2.4 at visible wavelengths), has led diamond to be primarily used in the jewelry and cutting and drilling industry.

Recently, the famous De Beers' synthetic CVD diamond manufacturer, Element Six has ventured in lab grown diamond for fashion jewelry (lightboxjewelry.com). Optically, diamond samples grown by CVD have the widest wavelength transmission spectrum known in material science, from 220 nm until the terahertz regime, and are therefore a suitable substrate for integrated photonic devices operable over a wide wavelength range for various technological applications (Fig. 4). The thermal conductivity value of diamond is 2000 W/mK, 5 times that of copper and is 100 times higher than typical optical materials, which has led to applications in thermal management for high power devices, and radiation detectors.

Chemical resistance allows CVD diamond components to operate in highly corrosive and hostile environments. The bio-inertness of CVD diamond allows its use in bio-sensing and in-situ medical and lab on a chip applications. Due to its extreme strength, diamond offers ultimate resistance to scratches and breakage. For applications targeting the NV properties of diamond, another important parameter to be considered is the intrinsic nitrogen concentration in the diamond. The two main grades of CVD diamond which are extensively used for laser writing experiments are, electronic grade CVD diamond (single crystal, Type A) with intrinsic nitrogen concentration of about 5 ppb and optical grade CVD diamond (single crystal, Type IIa) with a nitrogen concentration of about 100 ppb. For applications which require dense ensembles of NVs, diamond samples synthesized by high pressure-high temperature growth (HPHT, single crystal, Type Ib) with nitrogen concentrations of 100 ppm and above, are used.

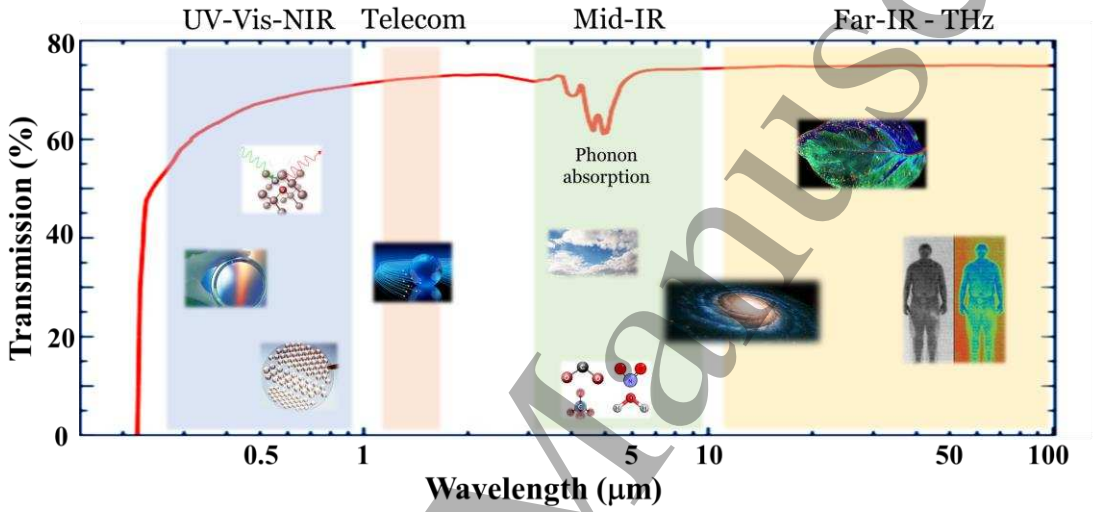

Fig. 4: Transmission spectrum of CVD diamond showing various applications depending on the wavelength range. Transparency in the UV-Vis-NIR region has been exploited to create diamond windows and lenses for optical systems. The NV excitation and collection wavelength range is in this region. The transparency in the telecom wavelength can be used for optical communications. The mid-IR transparency allows for applications in astro-photonics, molecular sensing and optical radar. The far-IR transparency which extends up to THz regime allows for applications in Far-IR astronomy imaging, bio-imaging, security screening and Terahertz waveguides for imaging applications. The transmission spectrum has not been corrected for reflection losses [70].

2. Femtosecond laser writing of photonics in the bulk of diamond

Here, we describe how femtosecond laser writing has enabled the first 3D photonics toolkit for diamond. In this method, focused ultrashort pulses are nonlinearly absorbed in the bulk of a transparent material, leading to a localized modification [34]. In glasses this modification is a refractive index increase which enables 3D waveguide writing [20,33] but in crystals, the lattice is damaged yielding a decrease in refractive index [71]. In addition, the formation of graphite during laser irradiation should be minimized to enable efficient waveguide devices. Below, we will describe how one can avoid these roadblocks to laser-induced waveguide formation in diamond to achieve photonic devices operational from the visible to the mid infrared.

2.1 Laser-induced bulk graphitic modifications

The study of pulsed laser induced modification in diamond was first performed in 1992 [72], applying 14 ns pulses from a frequency doubled Nd-silicate-glass laser (531 nm) focused onto type IIa diamond slabs, where a damage layer was created by deep ion implantation. Various techniques such as optical absorption, surface profilometry and channelling contrast microscopy were utilized for characterization of the laser irradiated spots. With increase in the incident laser power, three distinct regimes of modifications in the ion implanted regions were observed, namely, annealing, graphite layer formation and melting followed by graphitization. This pioneering work inspired the research by Kononenko *et al.* [73], in which, focused nanosecond excimer laser (248 nm wavelength) pulses were used for site-specific annealing of deuterium ion implanted diamond samples.

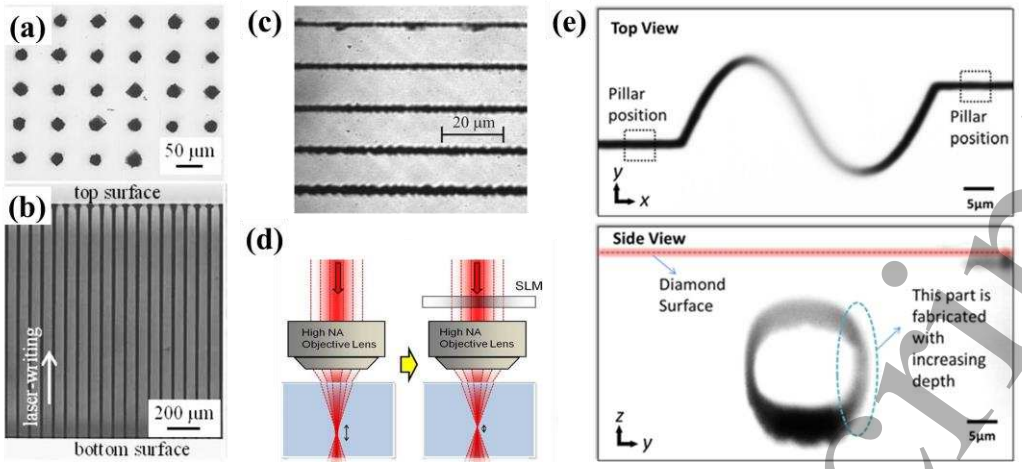

Fig. 5: (a) Overhead and (b) lateral optical microscope view of an array of laser induced modifications with 1 μJ of laser energy and 20 μm/s scan speed. The laser is focused from the top and the sample is translated along the laser propagation direction [74]. (c) Overhead optical microscope view of continuous graphitized tracks written by scanning the sample transversely with respect to the with scan speeds 30, 10, 5, 3 and 1 μm/s (from top to bottom) [75]. (d) Schematic showing the role of SLM in aberration correction to reduce vertical elongation of the laser-induced modification. (e) Top and the side view of spiral graphitic wire, laser written in the bulk of diamond employing an SLM to correct the elongation for different depths [76].

The first demonstrations of bulk femtosecond laser induced modification in diamond was performed by focusing 215 fs pulses at a repetition rate of 1 kHz from Ti:Sapphire amplified laser into single crystal diamond (type Ib, 3 mm × 3 mm × 1 mm) with pulse energy of 1 μJ using a 0.45 NA (20×) objective, creating vertical modifications by translating the sample with a scan speed of 20 μm/s along the direction of laser propagation [74]. Fig. 5(a) and Fig. 5(b) show the optical microscope image of the resulting tracks which had a diameter of 18 μm. Raman spectroscopy and electrical conductivity employed to study the material content of the laser induced tracks revealed formation of composite graphite, amorphous carbon and diamond like carbon [74].

Buried graphitic lines were laser written by focusing 140 fs pulses at a repetition rate of 1 kHz from a Ti:Sapphire laser into the bulk of single crystal diamond and by translating the sample transversely with respect to the beam with speeds from 1 μm/s to 30 μm/s, continuous graphitic lines were obtained [75,77], as shown in Fig. 5(c). However, the high refractive index of diamond (~ 2.4) leads to spherical aberration and hence an elongation of the laser-induced structures. Adaptive optical elements such as spatial light modulator (SLM) or deformable mirrors have been used to induce a phase correction onto the incident beam resulting in tighter focusing, [78] as depicted in Fig. 5(d). The use of adaptive optical elements has allowed the fabrication of conductive graphitic wires in arbitrary paths in 3D within the bulk of diamond [76], as shown in Fig. 5(e). Resistivity values, as low as 0.022 Ω cm, comparable with that of poly-crystalline graphite were obtained. Graphitic microstructures in diamond bulk have also been fabricated without sample translation by means of ultrashort Bessel beam laser writing [79]. Laser-written conducting graphitic wires have been used as electrodes in 3D diamond detectors for ionizing radiation detection [80–82].

2.2 Optimization of femtosecond laser-written structures for photonics

For photonic applications, graphite formation is detrimental because it absorbs visible wavelengths. Recently, the use of high repetition rate lasers for inducing bulk modifications in diamond has led to impressive results. Femtosecond laser writing in the bulk of diamond was performed by Eaton's group using a regeneratively amplified Yb:KGW system (Pharos, Light Conversion) with 230-fs pulse duration, 515-nm wavelength (frequency doubled) with variable repetition rate from 1 MHz to single pulse operation. Polished 5 mm × 5 mm × 0.5 mm synthetic single-crystal diamond samples (type II, optical grade with nitrogen impurities 100 ppb) acquired from MB Optics were used. High numerical aperture focusing objectives (NA > 0.7) were preferred in order to have higher resolution structures and additionally, the high NA objective allows lower pulse energies for writing, leading to reduced self-focussing.

Initial trials were focused on the creation of continuous modifications in the bulk of diamond using a repetition rate of 500 kHz. Fig. 6 shows the microscope images of the resulting structures written in the bulk of diamond by varying the pulse energy, scan speed and using three different objectives of 0.75 NA (Zeiss LD Plan-NEOFLUAR 63 ×), 0.95 NA (Olympus MPLAPON 100 ×) and 1.25 NA (RMS100X-O 100 × Olympus Plan Achromat Oil Immersion). The structures were formed at 50 μm depth, as measured from surface to the middle of structure.

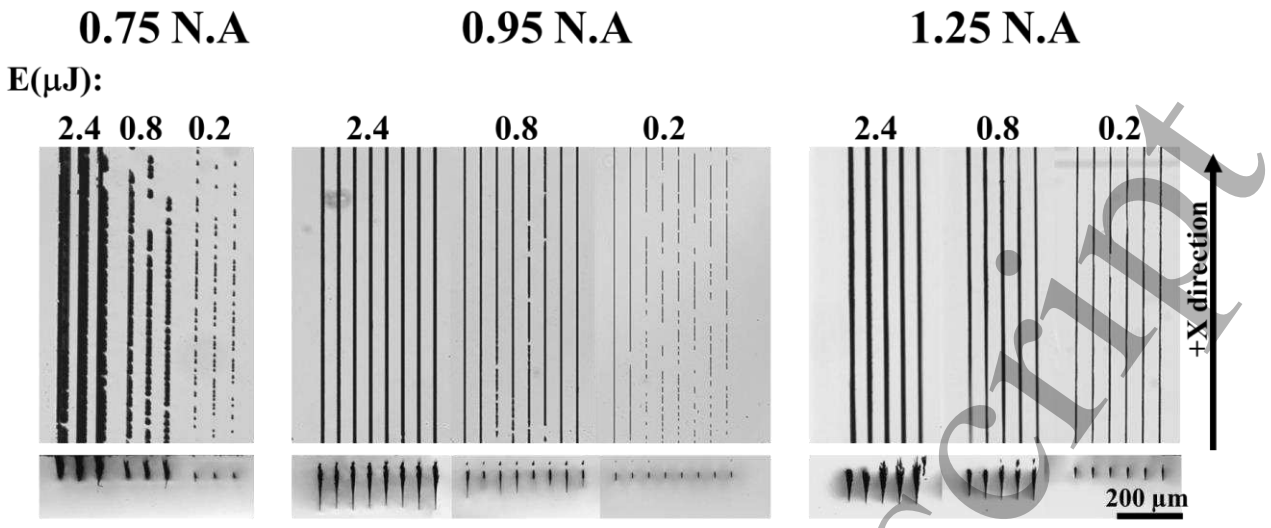

Fig. 6: Overhead and transverse optical microscope images of laser induced modifications in diamond using 0.75 NA, 0.95 NA and 1.25 NA focusing objectives (depth 50 μm). The scan speeds of laser writing (from left to right) in each energy sets of 0.75 NA are 0.05, 0.2 and 1 mm/s. For 0.95 NA, the scan speeds are 0.2, 0.5, 1 and 5 mm/s (written along, *+x* and *-x* directions (left and right), with *x* direction parallel to <110> crystallographic direction, as represented by the arrow) and for 1.25 NA, the scan speeds are 40, 50, 20, 5, and 2 mm/s.

It is immediately apparent from Fig. 6 that higher NAs led to smoother and more continuous laser-written bulk structures. For all three tested microscope objectives, higher energies (> 1 μJ) produced strongly elongated modifications, and also creating non-uniform structures at lower scan speeds as can be seen in Fig. 6. The structures written with 0.75 NA were discontinuous for lower energies (< 1 μJ) while higher energies (> 1 μJ) led to surface ablation. The 0.95 NA objective produced continuous modification for higher energies (> 1 μJ), but the resulting structures were elongated and asymmetric. 1.25 NA was identified as the optimum microscope objective for bulk laser writing in diamond, as it led to continuous and smooth modifications even at low energies and for a wide range of scan speeds, as shown in Fig. 6. The polarization of the laser beam was not found to have a noticeable effect on the modification lines. The favoured conditions for producing uniform and repeatable modifications in the bulk of diamond with 1.25 NA objective were found to be a repetition rate of 500 kHz, a pulse energy of 100 nJ, and a scan speed of 0.5 mm/s. Studies performed on the effects of directionality show a non-reciprocal feathering effect while fabricating along <100> crystallographic direction with low repetition rate femtosecond laser to create graphitic wires [83].

Micro-Raman analysis performed on the laser written tracks helped to elucidate the structural modification within the laser induced modifications in the bulk of diamond [84,85]. Micro-Raman spectra were recorded with a laser excitation source of wavelength 532 nm.

Fig. 7(a), (b) and (c) show the results from the micro-Raman studies performed on the laser induced modification written with the optimum parameters described above. The Raman signal obtained from within the modification compared with the signal obtained from the pristine showed a reduction in the intensity of the diamond peak at 1333 cm^{-1} by about 15%. The appearance of G peak at 1575 cm^{-1} and the D peak at 1360 cm^{-1} suggest the transformation of sp^3 bonding into sp^2. The widths of the G peak being greater than 100 cm^{-1} and the ratio of the intensities, I(D)/I(G) being close to 1, suggests that the sp^2 clusters are mainly composed of amorphous carbon phase rather than graphite [86]. Raman analysis performed on lines written with lower repetition rates of 25 kHz and 5 kHz, keeping the pulse energies constant at 800 nJ, showed the G peak becoming sharper as the repetition rate was reduced, indicating increased graphitization.

High resolution transmission electron microscopy (TEM) and electron energy loss spectroscopy (EELS) performed by Patrick Salter's group on thin FIB milled cross section areas of the laser written tracks showed a non-uniform structural modification consisting of about 4% of sp^2 bonded carbon [87], as shown in Fig. 7(d) and (e). The tracks were written using a femtosecond Ti:Sapphire laser at 1 kHz repetition rate focused 4 μm beneath the surface. An SLM was employed to correct for aberrations. Despite the low composition of sp^2 carbon, the laser written wires have shown good conductivity [76].

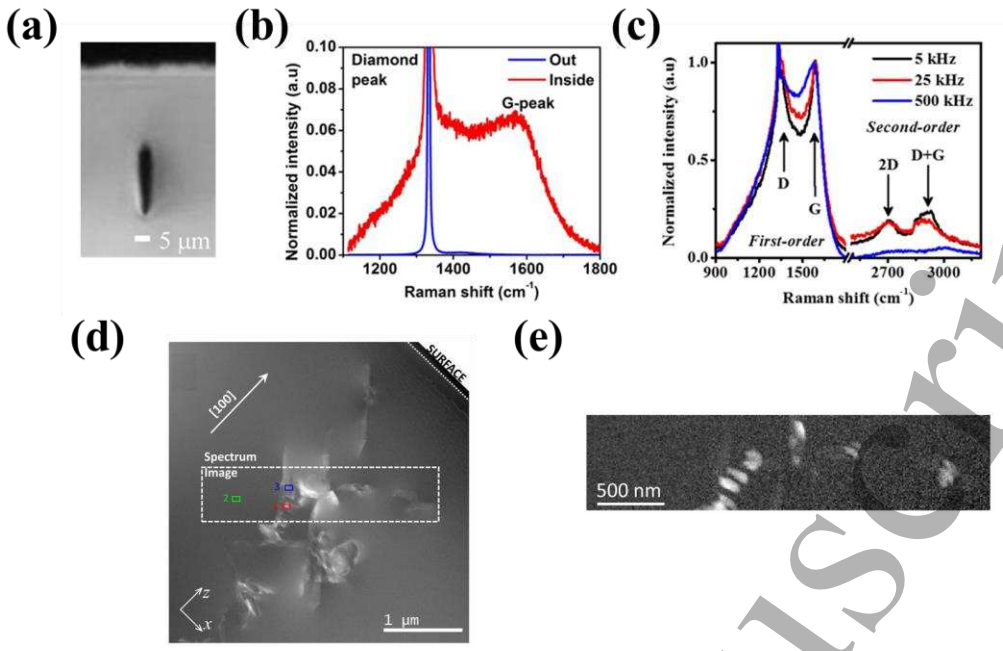

Fig. 7: (a) Transverse optical microscope image of a single laser-induced track written with 515 nm wavelength, 500 kHz repetition rate, 100 nJ pulse energy, 0.5 mm/s scan speed, 50 μm depth and 1.25 NA lens. (b) Micro-Raman spectra captured within the laser written track and the pristine diamond. The spectra were normalized to the diamond Raman peak. (c) Micro-Raman spectra (normalized to the G-peak) in the center of the modification tracks written with repetition rates of 5, 25 and 500 kHz, with pulse energy being constant (800 nJ) [85]. (d) Scanning transmission electron microscopy (STEM) image of FIB milled cross section of laser induced tracks [87]. (e) Spatial distribution of sp^2 bonding in the cross-sectional region defined as 'image' in (d).

2.3 Femtosecond laser writing of bulk optical waveguides for the visible wavelengths

The material characterization revealing the negligible presence of graphite in the laser induced modification is an encouraging result to extend laser writing to inscribe complex photonic components in bulk diamond. Although, type I waveguides in diamond would be preferred for photonic networks in diamond, there is a narrow range of pulse energies for gentle positive refractive index change over amorphization and hence makes it a challenging to fabricate. Hence, the type II modality of laser writing was exploited to create the first waveguide in the bulk of diamond using femtosecond laser writing [85]. Two lines written with 100 nJ pulse energy, 0.5 mm/s scan speed, 500 kHz repetition rate, 1.25 NA focusing, 515 nm wavelength, and spaced by 13 μm create a stress in the region between them, confining the optical mode at visible wavelengths. The waveguides were formed 50 μm below the surface and were characterized employing a fiber coupling strategy at 635 nm, revealing an insertion loss of 6 dB for a 5 mm long waveguide with a mode field diameter (MFD) of about 10 μm × 10 μm, as shown in Fig. 8(a). A 532 nm wavelength laser light was launched into the waveguide while the output mode was collected using a spectrometer after filtering the excitation 532 nm using a notch filter. The spectral properties thus obtained from the NVs within the waveguide showed the characteristic photoluminescence spectrum with the ZPL at 637 nm [85].

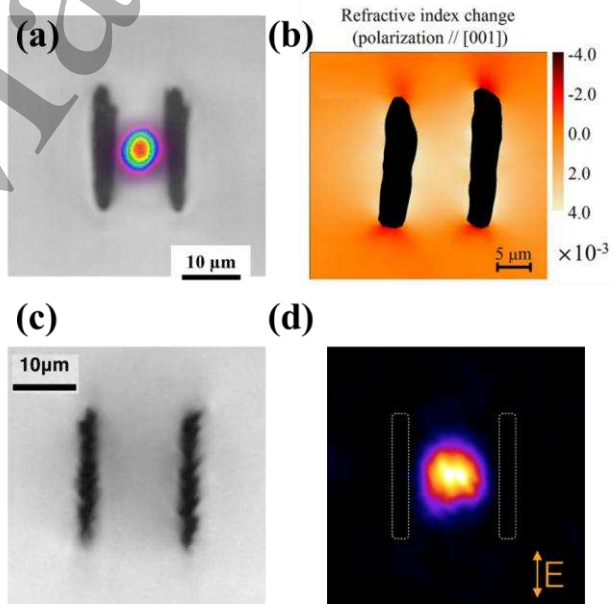

Fig. 8: (a) Transverse optical microscope image of type II waveguide with a separation of 13 μm with the optical guided mode at a wavelength of 635 nm in the inset [85]. (b) A map of refractive index variation of the waveguide shown in (a), deduced by performing polarized micro-Raman studies ([001] crystallographic direction is taken along the vertical axis) [88]. (c) Transverse optical microscope image of Type II waveguide written in diamond employing an SLM to form the long vertical wall structure composed of multiple dots scanned along the sample. (d) Optical guided mode along the waveguide shown in (c) at a wavelength of 780 nm launched using a polarization maintaining fiber [89].

The waveguides supported only TM guiding, the reasons for which are described below. The effect of the repetition rate on the central diamond region of the type II waveguides showed that the crystal disorder in the guiding region is higher for lower repetition rate when the tracks are written without the use of an SLM [84], as can be inferred from Fig. 7(c).

Salter's group demonstrated the ability to write waveguides with a Ti:Sapphire femtosecond laser having a repetition rate of 1 kHz, aided by an SLM [89]. The SLM yielded nearly symmetric structures (1 μm transversely × 2 μm vertically) when focused with 1.4 NA oil immersion lens, and a multiscan writing procedure with six consecutive scans separated vertically by 3 μm was applied to form vertically elongated side walls (Fig. 8(c)), similar in geometry to those of Eaton's group. The type II waveguides were formed with 30 nJ pulse energy, 0.1 mm/s scan speed at 50 μm depth, with a transverse spacing of 17 μm, and designed for single-mode operation at 780 nm wavelength (Fig. 8(d)), having an insertion loss of 4 dB for 3 mm long waveguide.

To probe the guiding mechanism within the type II waveguide structure, polarized micro Raman has been employed on laser written structures shown in Fig. 8(a). By correlating the polarized Raman signal to the stress matrix around the type II waveguide structure, and considering the piezo-optic tensor of diamond, a refractive index profile map was developed, as shown in Fig. 8(b), for TM polarization. A positive refractive index change, $\Delta n = 3 \times 10^{-3}$ at the waveguide center has been inferred [88]. For the TE polarization, the refractive index decreases in the guiding region, explaining the TM-only guiding behaviour of the waveguides. Waveguides supporting both TM and TE polarizations have been laser written by engineering the structure to be symmetric in both transversal directions[89].

2.4 Femtosecond laser writing of bulk optical waveguides for Infra-red wavelengths

The wide transparency of diamond makes it a promising photonic platform for visible, mid-IR and even extendable to terahertz wavelength regime. Waveguides with larger separation have been laser written for guidance of near - IR, telecom and mid-IR wavelengths using a high repetition rate of 500 kHz and without the use of an SLM.

Waveguides with a spacing of 15 μm supported single mode guiding for 808 nm wavelength with a mode field diameter of 8.5 μm × 10 μm and with a spacing of 19 μm, the waveguide supported single mode guiding for 1550 nm with a mode size of 16 μm × 21 μm [84]. Waveguides with larger separations of 30 μm and 40 μm have been shown to guide wavelengths of 2.4 μm and 8.7 μm respectively, which are promising for applications in molecular sensing, optical radar and astro-photonic applications [90]. Fig. 9 shows the optical microscope images and modes of the various waveguides discussed.

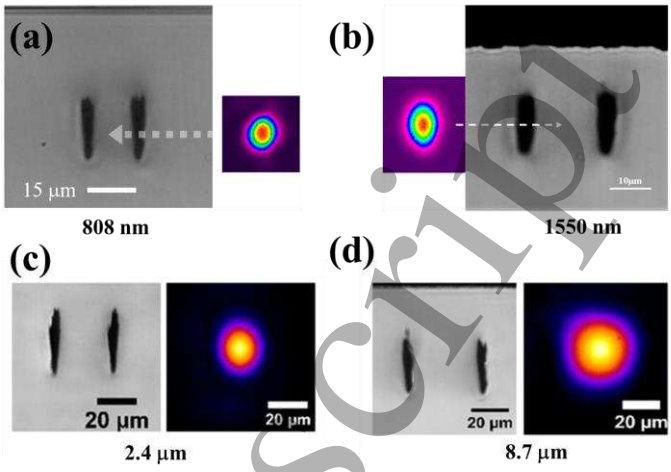

Fig. 9: Transverse optical microscope images of type II waveguide with a separation of (a) 15 μm, (b) 19 μm, (c) 30 μm and (d) 40 μm with the optical guided mode at wavelengths of (a) 808 nm, (b) 1550 nm [84], (c) 2.4 μm and (d) 8.7 μm [90].

2.5 Femtosecond laser writing of advanced photonic components

The successful operation of the laser inscribed waveguides paves the path towards more complex photonic networks in diamond. The use of an SLM grants the ability to create structures in 3D within the bulk of diamond. Employing a feedback loop between the translational stage and the phase mask on the SLM, 50:50 Y splitters have been laser written by the group of Salter, using a repetition rate of 1 kHz, with the two arms of the Y being separated in the z direction as shown in Fig. 10 (a) [89].

Narrow band reflection elements in diamond allowing wavelength selective filtering are instrumental in quantum information [91], magnetometry [92] and Raman laser applications [93]. In a collaborative effort between the Salter and Eaton groups, femtosecond laser writing was applied to create Bragg grating waveguides in diamond [94]. A Ti:Sapphire femtosecond laser operating at 1 kHz was used to write the type II waveguide employing an SLM. The same micromachining workstation was used to form a periodic structure above the type II modification and hence creating a modulation of refractive index along the length of the waveguide. Fig. 10(b),(c) show the microscope image of the resulting structure. The periodicity set to 1.3 μm resulted in a 4th order Bragg reflection at around 1550 nm. A transmission dip of 6.5 dB was observed, as shown in Fig. 10(d). The corresponding reflection spectrum is shown in Fig. 10(e). The reflection spectrum was calibrated using out-of-band Fabry-Perot fringes due to Fresnel reflections. Periodic structures with reduced spacing would allow Bragg waveguides operational in visible wavelengths for the integration of NVs.

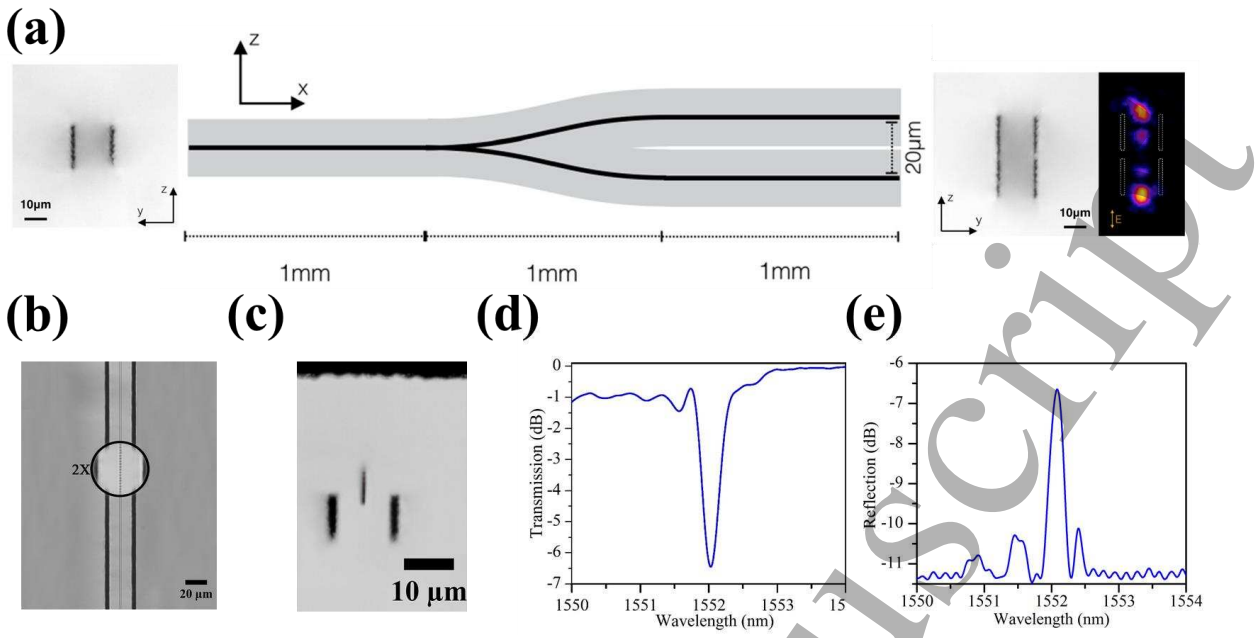

Fig. 10: (a) A schematic of the laser written 50:50 Y splitter in bulk of diamond. A transverse optical microscope image of the input facet is shown on the left and the output facet along with the mode profile is shown on the right [89]. (b) Overhead and (c) transverse optical microscope image of Bragg grating waveguides fabricated in diamond showing the periodic modifications within the Type II structure. (d) Transmission and (e) reflection spectrum of the Bragg grating waveguide [94].

3. On demand creation of NVs using femtosecond laser pulses

3.1 Static exposure modifications in diamond

One of the primary challenges for integrated diamond quantum photonics is the placement of color center defects in the bulk. The conventional technique of deterministic NV center placement is based on ion implantation followed by thermal annealing [95,96]. Although the method is capable of submicron spatial accuracy, the high energies required for deep NV creation causes damage at the irradiated sites and degrades the spectral properties of the NV centers [97].

In a more recent work, femtosecond laser pulses have been used to form single NVs in the bulk of electronic grade diamond [98]. The method is based on creation of vacancies in the bulk of diamond using a single focused femtosecond laser pulse. When followed by annealing at temperatures above 600°C, the vacancies are mobilized and can be captured by substitutional nitrogen impurities, which are randomly distributed in the bulk of diamond [95], as depicted in Fig. 11(a). In this pioneering work, electronic grade diamond sample with an intrinsic nitrogen content of less than 1 ppb was used. A single femtosecond laser pulse was focused 50 μm below the surface of diamond with pulse energies between 16 to 62 nJ. Using an SLM, the phase profile of the beam was corrected for spherical aberration due to the refractive index mismatch between the focusing objective/immersion oil and diamond. Twenty identical spots for each pulse energy were written to study the statistics of single NV creation. The laser written spots were annealed at a temperature of 1000°C for 3 hours in a nitrogen atmosphere to avoid oxidation at the diamond surface. This temperature was chosen based on previous work showing that high annealing temperatures improve the properties of the resulting NV centers [99].

Confocal fluorescence microscopy revealed bright photoluminescence from the laser written sites, as shown in Fig. 11(b). Additionally, by comparing the position of the fluorescent sites with the laser irradiated area, an accuracy of placement of about 100 nm was inferred. Obtaining such impressive resolution for a depth of 50 μm is a challenging task with ion beam implantation due to the straggling effects associated with high energy implantations and also leading to creation of large number of NVs along the focus [97]. For certain sites, the second-order intensity correlation performed on the emitted photons showed the $g^{(2)}(0) < 0.5$ indicating single photon emission, as shown in Fig. 11(c). For a pulse energy of 26 nJ, about 50% of the laser irradiated spots were single NVs. Additionally, Hahn-Echo measurements performed on the spots showed the spin decoherence times (T_2) to be between 30 and 80 μs, as shown in Fig. 11(d), comparable with the T_2 times from ion implanted NVs [100]. The use of SLM has enabled the fabrication of a 3D array of NVs in the bulk of diamond [101]. More rigorous characterization compared to the initial study revealed impressively high spin coherence times up to $T_2 = 800$ μs for the laser written single NVs.

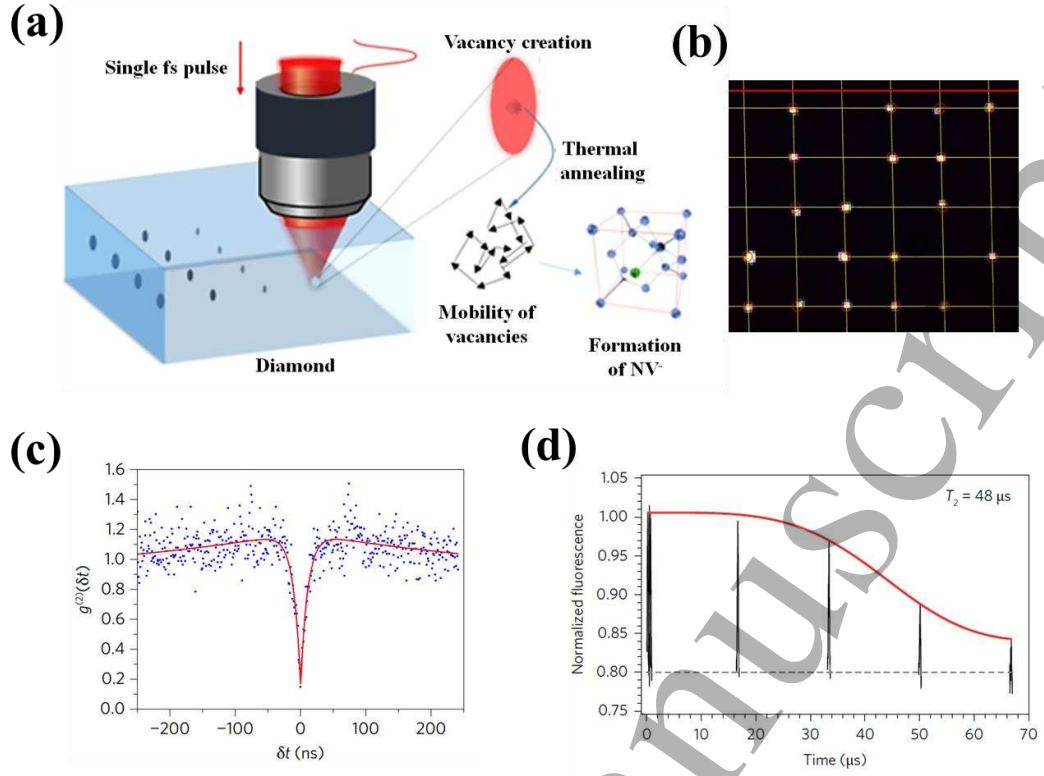

Fig. 11: ***(Electronic grade diamond)*** (a) Schematic depicting laser writing of NV color center in diamond. The focused femtosecond laser pulses create vacancies which when annealed at high temperature, gets mobilized and captured by substitutional nitrogen atom to form a single NV center. (b) Photoluminescence from laser written NV centers with the red circles indicating the laser focused spot, revealing the accuracy of placement. (c) Second order intensity correlation spectrum from the laser written NV, showing $g^{(2)} < 0.5$ indicating single photon emission. (d) Room temperature Hahn echo data for an NV centre created with pulse energy of 20 nJ, fitted with the function, $I(\tau) = y_1 e^{-(\tau/T_2)^n} + y_0$, where the exponent n is a free parameter and y_0, y_1 and T_2 are fitting parameters [98].

A concurrent study was performed by Eaton's group, on laser writing of NVs within the bulk of both optical and electronic grade diamond without the use of an SLM. The initial trials were performed in optical grade diamond sample with a nitrogen content of about 100 ppb with the aim of creating ensemble of NVs for optical magnetometry and electrometry. Second harmonic 515 nm wavelength femtosecond laser pulses from a Yb:KGW fiber laser with pulse energies from 2 nJ to 100 nJ, and pulse numbers from 1 to 5000, were focused using a 1.25 NA objective at a depth of 25 μm within the bulk of the diamond substrate. The static exposed sites were separated by 20 μm, offering a convenient spatial separation for subsequent characterizations.

Preliminary overhead microscope imaging of the static exposures revealed a formation of visible dark modification for higher energies (> 30 nJ) and higher pulse numbers (≥ 5), as can be seen in Fig. 12(a). The sample was subsequently annealed at 1000°C for 3 hours. Confocal photoluminescence studies using 532 nm excitation wavelength, with the setup described in Sotillo *et al.* [84], were performed on the static laser exposed positions. The morphology of the laser-written exposures in Fig. 12(a) was unchanged after the thermal annealing treatment.

Three different regimes were found for the laser written spots depending on the laser net fluence. The laser net fluence (NF), is the product of the pulse number N and per-pulse fluence F_p, and represents the total laser exposure. For the static exposures creating visible marks i.e., high energy and high pulse numbers, the photoluminescence showed the presence of a G-peak before and after annealing, as shown in Fig. 12(b) and the ZPL of NV was not recovered after annealing. This implies that the laser interaction produced amorphization in the visible laser-written exposures, suggesting that the laser net fluence was too high. The photoluminescence performed for low energy (<10 nJ) static exposures showed no significant change in the ZPL intensity of NV or the Raman peak before and after the annealing, as shown in Fig. 12(c). Such pulse energies are too low to create NVs within the laser focal volume.

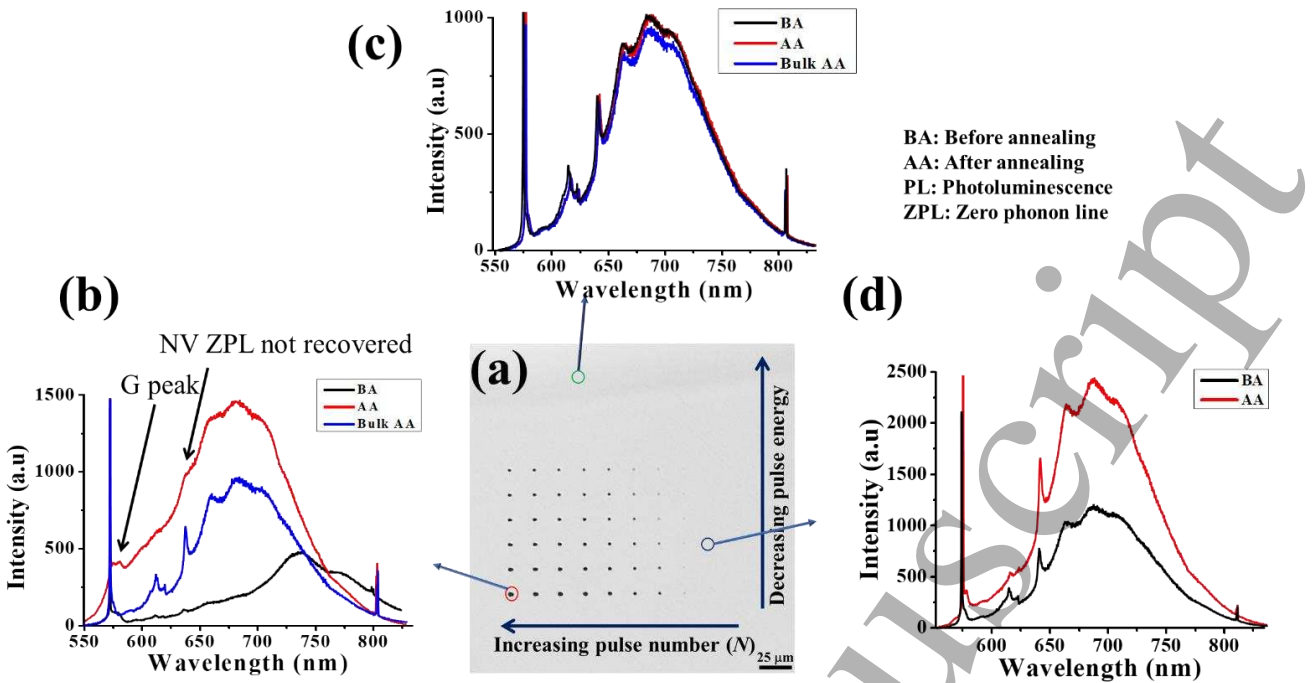

Fig. 12: ***(optical grade diamond)*** (a) Overhead microscope image of laser induced modification for pulse energies of 2, 6, 10, 20, 30, 40, 50, 60, 80 and 100 nJ with pulse numbers (N) of 1, 5, 25, 50, 100, 500, 1000, 2000 and 5000 at a depth of 25 µm. A typical confocal photoluminescence measured from (b) visible modifications formed with E_p > 30 nJ for $N \geq 5$, (c) invisible static exposures with E_p < 30 nJ for all values of N and (d) invisible static exposures with E_p > 20 nJ and N =1.

The sweet spot for laser writing of NVs in optical grade diamond was for pulse energies of E_p > 20 nJ with a single pulse. The photoluminescence from such static exposures, after annealing, showed an enhancement in the NV signature photoluminescence (600 nm – 750 nm), without any presence of G-peak, as shown in Fig. 12(d). This result indicates the presence of NV centers within the static exposures with good spectral properties and lower amorphization. These experiments show that single pulses are required to avoid amorphization and damage of the crystal lattice, and there is a range of pulse energies which can be tuned to control the concentration of laser-formed NVs. It must be noted that the exact pulse energy to create NVs with good spectral properties would depend on the intrinsic random distribution of nitrogen within the sample, which varies from sample to sample and also within different regions of the same sample. The Eaton group is currently studying the formation of NV within optical grade and HPHT diamond, with the goal of creating a high concentration ensemble of NVs, benefitting optical magnetometry [102] and electrometry [103].

Based on the feedback from the laser writing of NVs in optical grade diamond, Eaton's group studied the formation of single NVs in electronic grade diamond without the use of an SLM. Single femtosecond laser pulses were focused 30 µm below the surface of the diamond sample with a 1.25 NA oil immersion objective, using pulse energies between 10 and 30 nJ [84]. Since approximately 100-1000 nitrogen impurities are contained within the focal volume of the laser beam (~ 1 μm^3), the probability of forming a vacancy in the neighbourhood of a nitrogen atom is lower than the optical grade sample (20000-200000 nitrogen atoms in focal volume) and therefore, the chance of creating a single NV is higher. The resulting static exposed sites were invisible under white light optical microscopy. Following the static exposures, the sample was annealed at 1000°C for 3 hours. Confocal fluorescence microscopy was performed on the spot written with an energy of 24 nJ, which showed a spatial confinement of less than 1 μm^2, as shown in Fig. 13(a). Photoluminescence spectra acquired at the static exposed sites revealing the signature ZPL from NV, as shown in Fig. 13(b).

Second-order intensity correlation measurements performed on the sites, showed single photon emission with $g^{(2)}(0)$ < 0.5 indicating single photon emission, as shown in Fig. 13(c). Statistical analysis was performed on 80 laser written spots of varying pulse energies from 20 to 30 nJ. Fig. 13(d) shows the probability of forming single or multiple NVs for varying pulse energies, averaged over the measured set [104]. The single NV center formation probability increases with pulse energy, however as the energy increases more, the probability of formation of multiple NV centers at the same site also increases. At 30 nJ, multiple NV center formation appears to dominate. However, it should be noted that the formation probability is also dependent on the local density of nitrogen which can vary between samples and even between different sections of the same sample.

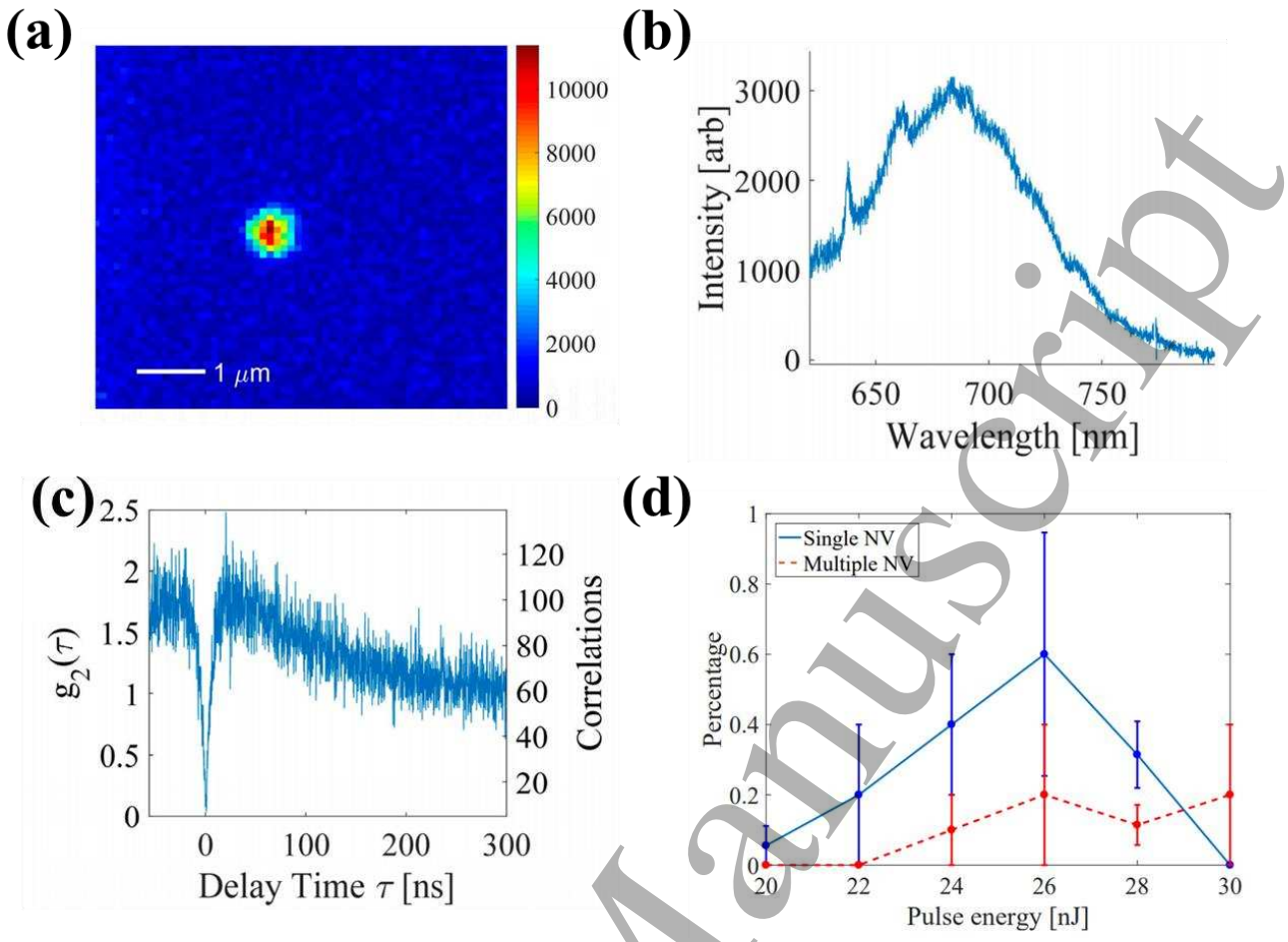

Fig. 13: ***(Electronic grade diamond)*** (a) Overhead photoluminescence map of static laser exposure with a pulse energy of 24 nJ followed by 3-hour annealing treatment at 1000°C. (b) The room temperature confocal photoluminescence spectrum of the 24 nJ static exposure NV. (c) Intensity autocorrelation (corrected for background on left *y*-axis, raw uncorrected correlations count on the right *y*-axis) of the laser exposed spot revealing single photon emission[84]. (d) NV center formation statistics showing the probability of obtaining single NV and multiple NV centers for increasing pulse energy of the incident laser beam [104].

3.2 Laser induced vacancy diffusion

The thermal annealing performed on the diamond substrate after laser irradiation leads to random diffusion of the laser created vacancies followed by statistical probability of NV center creation. This probabilistic creation leads to a relatively low yield and low positioning accuracy of NV center formation. To address these problems, Chen *et al.* [105] recently proposed that a train of low energy focused femtosecond laser pulses can be used instead of the thermal annealing treatment, to selectively induce vacancy diffusion at the laser exposed sites.

First, an initial laser pulse of energy 27 nJ, called the seed pulse from a Ti:Sapphire femtosecond laser with a central wavelength of 790 nm operating at 1 kHz repetition rate was focused into the bulk of single crystal, type Ib, HPHT diamond with an intrinsic nitrogen concentration of 1.8 ppm, using a 1.4 NA objective. The seed pulse is responsible for creating an ensemble of vacancies within the focal volume. Following the seed pulse, a train of 1 kHz pulses typically for a duration of few seconds, with lower 19-nJ pulse energy, referred to as the diffusion pulses, was focused into the same spot. A live monitoring of the fluorescence emission from the spot is performed by a confocal setup using a 532 nm excitation laser and spectral filters to observe the NV signature wavelength range of 650 nm to 750 nm. The train of diffusion pulses was stopped when the NV signal was observed by the confocal imaging, indicating the creation of a single NV. Using the above-mentioned method, high quality NV centers with a yield of 96% and about 50 nm positioning accuracy have been fabricated in HPHT diamond. Adopting MHz repetition rate femtosecond laser for vacancy diffusion should enable more efficient creation of single NVs, particularly in electronic grade samples with lower nitrogen impurity levels.

Based on the plot of fluorescence intensity with respect to the duration of illumination by the diffusion pulses, a 4-step theory to explain the dynamics of creation of NVs using laser induced diffusion has been proposed. The four steps are

summarized as follows. (i) The seed pulse generates a vacancy (V) and the split interstitial (I) which form the Frenkel defect. The created vacancy being lattice depletion is surrounded by negative strain whereas split interstitial and the substitutional nitrogen (N) are surrounded by positive strain. (ii) The diffusion pulses of 19 nJ mobilizes V and I and not N due to the lower activation energies of V and I. V attracts N and I, but N and I repel each other, due to the positive and negative strain. The V and I which are formed away from substitutional N diffuse or combine back. (iii) Due to the lower stability energy, the V formed near N stays in between N and I, resulting in intermittent NV fluorescence emission peaks observed in this time scale. (iv) The strong attractive force between N and V results in the diffusion of I, resulting in single NV formation. Further illumination of the diffusion pulses will result in the creation of multiple NVs and NV complexes.

4. Femtosecond laser inscribed integrated quantum photonic chip in diamond

4.1 Single NV coupled to waveguide

The ability of the femtosecond laser writing to create optical networks, and to deterministically place the NV centers in the bulk of diamond, allows one to create integrated quantum photonic device in which laser written waveguides are coupled with laser fabricated NVs.

In this endeavour pursued by Eaton's group, type II waveguides with a spacing of 13 μm, at a depth of 25 μm have been laser written in ultrapure electronic grade diamond, using a writing wavelength of 515 nm, repetition rate of 500 kHz, scan speed of 0.5 mm/s, pulse energy of 60 nJ and a 1.25 NA focusing objective. The waveguides exhibited single mode guiding at 635 nm with an MFD of 9.5 μm and a propagation loss of 4.2 dB/cm. Aiming towards an integrated waveguide – NV device and considering that thermal annealing is required to form the NV centers in diamond, the effect of heat treatment on the laser formed waveguide was first investigated. Type II waveguides written in other crystals have been shown to get erased with high temperature annealing [106,107]. In order to study the effect of high temperature annealing on laser written waveguides in diamond, micro-Raman analysis was employed.

Micro-Raman spectra were obtained from the central guiding region between the two modification lines and from within the modification lines induced by the waveguide, before and after the 1000°C, 3-hour annealing. For the central guiding region, the width and the shift of the diamond peak remained unaltered before and after annealing as shown in Fig. 14(b). The peak was slightly shifted away from the pristine diamond Raman shift at 1333 cm^{-1}, due to the stress induced by the type II lines. The micro-Raman spectrum from the laser induced modification showed the narrowing of D peak and G peak at 1360 cm^{-1} and 1575 cm^{-1}, respectively after annealing, as shown in Fig. 14(c). This narrowing is attributed to the formation of nano-crystalline graphite [108]. Similar behaviour was observed with high temperature annealing of ion implanted diamond structures [109]. The mode profile and the insertion losses of the waveguide remained unchanged with annealing, suggesting that the temperature required to degrade the waveguide is higher than the annealing temperature needed for NV formation. Additionally, the waveguides have been observed to be stable over months of measurements, even with regular acid cleaning and low temperature (4K) measurements, without any photo-bleaching effects and thus establishing the robustness of the laser written photonic circuits in diamond.

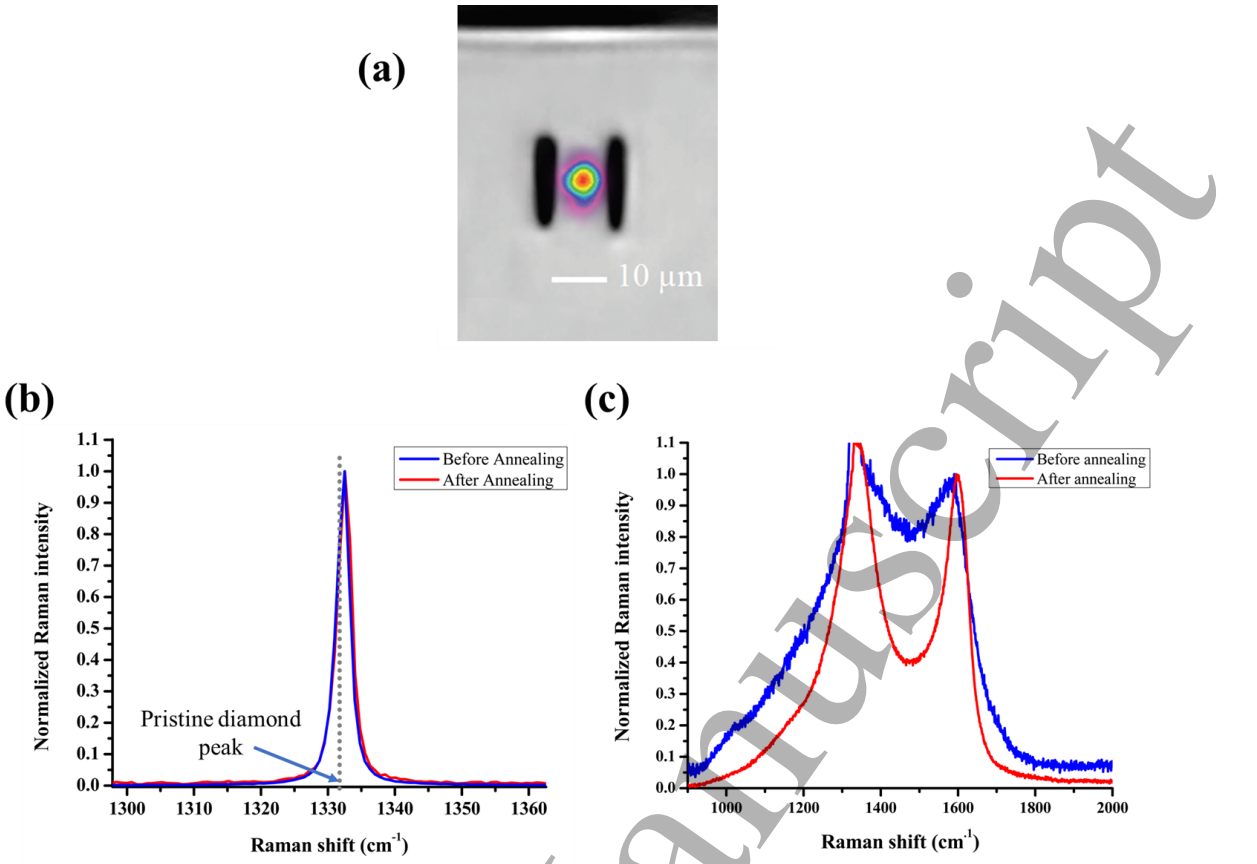

Fig. 14: ***(Electronic grade diamond)*** (a) Transverse optical microscope view of the type II waveguide with the guided mode at 532 nm shown in the inset. Comparison of the Raman shift before and after annealing for (b) the central guiding region between the two modification lines and (c) within the modification line induced by laser.

The integrated device consisted of the laser written waveguide with the parameters mentioned earlier, followed by static exposures of single femtosecond laser pulse with an energy of 28 nJ at 5 different spots within the center of the waveguide length, separated by 20 µm from each other at a depth of 25 µm, as shown in Fig. 15(a). Considering the resolution of NV placement (which is about 100 nm) and the focal spot diameter of the laser beam in the bulk diamond (which is about 1 µm), NVs can be placed with a spacing of a few µm separation using laser writing. For interaction between the NVs, a separation distance of few tens of nanometers will be necessary[110]. Although nanometric spacing is possible with multiple NVs produced by a single static femtosecond laser exposure, the process is stochastic. Hence, it will be beneficial to create separate NVs coupled to several nuclear spins with external coupling through laser induced waveguides for excitation and collection of NV signal[91]. Marker points formed with 25 pulses and a pulse energy of 100 nJ, were written outside the waveguide for easier identification of the laser written spots within the waveguide. The same laser micromachining workstation used for both the waveguide and the NV creation allows for sub-micrometer alignment with respect to each other. The sample was annealed at 1000°C for 3 hours.

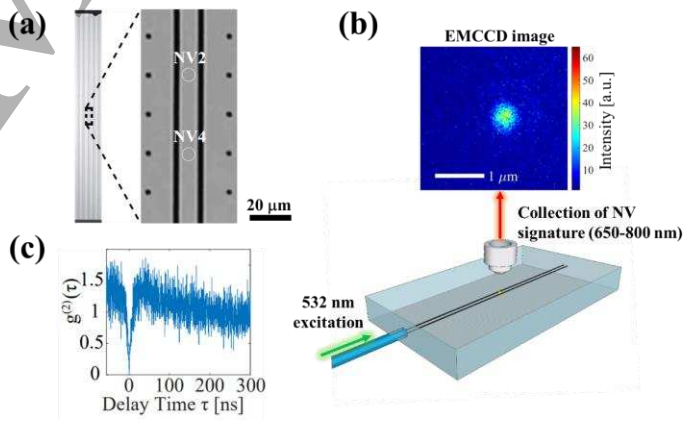

Fig. 15: ***(Electronic grade diamond)*** (a) Overhead optical microscope view of the entire 2 mm long waveguide along with the zoomed in view of the central region consisting of the 5 static exposures. The two spots which showed NV emissions are marked as NV2 and NV4. (b) Schematic showing 532 nm excitation wavelength launched using fiber coupling into the laser written waveguide to excite the NV formed within (shown as a yellow sphere within the waveguide), and the photoluminescence image collected from the NV using overhead microscope objective onto an EMCCD. (c). Intensity autocorrelation performed on NV2 revealing single photon emission [111].

Using the characterization setup described in Hadden et al. [111], initial photoluminescence imaging performed on the waveguides showed single NV emission from 2 out of the 5 spots, represented as NV2 and NV4 in Fig. 15(a). NV2 was chosen for further characterization. By launching 532 nm excitation wavelength using fiber coupling into the laser written waveguide, the NV2 emission was collected using overhead microscope objective onto an electron multiplying charge-coupled device (EMCCD), as shown in Fig. 15(b). The integrated device allows for easy compatibility with existing optical fiber technology. The second order intensity correlation measurements performed on the laser written NV showed single photon emission, as shown in Fig. 15(c).

4.2 Ensemble NV creation

The characteristics of single NVs, which make them an interesting quantum resource for quantum communication and computation, also open up the opportunity for high resolution or high sensitivity magnetometry and electrometry. As an electronic spin system with uniquely long room temperature coherence time, it is also sensitive to magnetic and electric fields which change the transition energy between its spin states. These shifts may then be read out optically by monitoring the spin dependent fluorescence rate, as the frequency of a microwave field is tuned across the transitions.

Atomic force microscopy based magnetometry using single NVs in nano-diamonds or within special fabricated diamond tips has been employed to push the spatial resolution of this type of magnetometry to the nanoscale [112]. However, the speed of the measurement (or equivalently the sensitivity in a fixed time) is limited because it is based on the measurement of a single NV. Sensing based on ensembles of NVs allows for much faster measurement (or higher sensitivity) for the sacrifice of nanoscale spatial resolution. The simultaneous measurement of each member of an ensemble of size M gives a $\sqrt{M}$ improvement in the sensitivity, although for extremely high densities of NVs, the enhancement can become offset by a reduction in the NV coherence time though interaction with closely spaced paramagnetic defects [92]. Thus, the key is to produce high enough densities of NVs to improve the detected fluorescence rate, without negatively affecting their coherence times. For ion implanted NVs it seems that a sweet spot exists at an NV density of around 2×10^{16} cm^{-3} [113].

Sensing based on thin layers of ensemble NVs produced at the surface of diamond through ion implantation has already been demonstrated allowing for example the measurement of single neuron action potentials [114]. Meanwhile, broadband magnetometry and electrometry based on much larger ensembles within ion irradiated or naturally NV rich bulk diamond samples has allowed for even higher sensitivities [103,113]. Femtosecond laser writing presents the opportunity to produce high density NV ensembles coupled to advanced elements such as optical waveguides, Bragg reflectors and microfluidic channels. Such devices will open the way for high sensitivity lab on chip devices for life sciences.

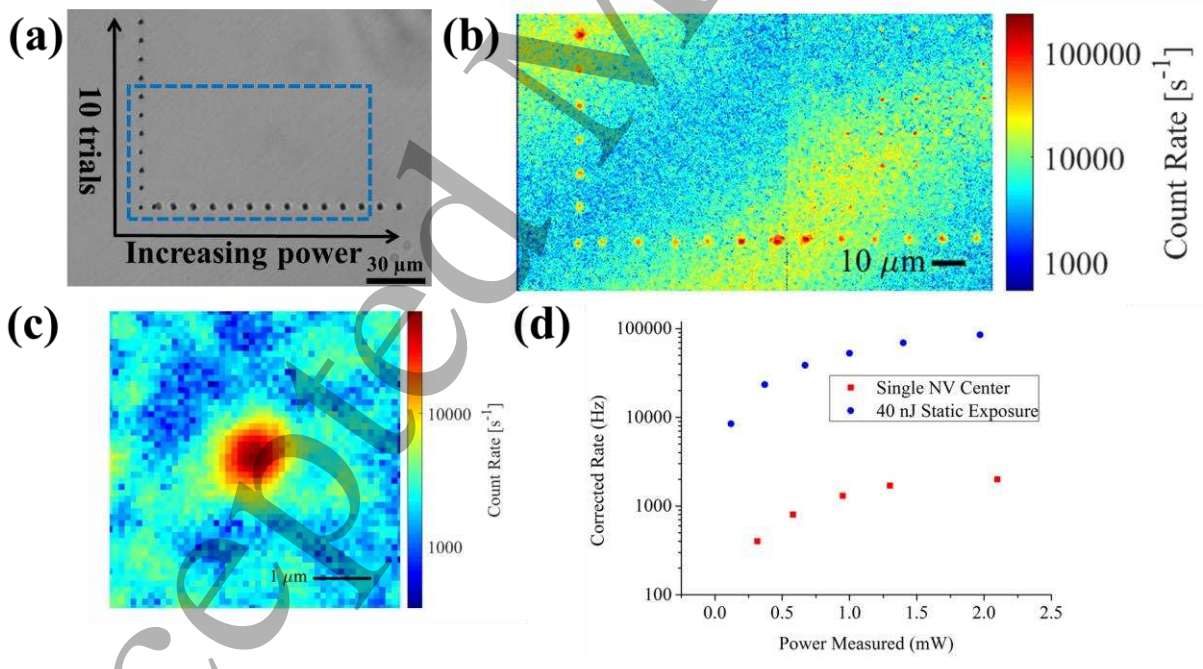

Fig. 16: ***(Optical grade diamond)*** (a) Optical and (b) room temperature confocal microscope image of an area of optical grade diamond sample written with single pulse static exposures with pulse energy 10 nJ to 60 nJ. Markers visible in the optical microscope are written with 25 pulses of pulse energy 100 nJ to identify the static exposure area. c) Zoomed in confocal scan of 40 nJ static exposure. d) Saturation measurement showing ~ 50× increase in detected count rate from the peak of the laser written spot as compared to a single NV in the same sample.

Initial investigations by the Eaton group on the femtosecond laser writing of high-density NV ensembles were performed utilizing the techniques presented in Section 3 and Section 4, for the production of single NV centers. However, in order to increase the density of NVs produced, diamond samples with higher initial substitutional Nitrogen content were used. An optical grade (~ 100 ppb N) diamond was written with single static exposure femtosecond laser pulses with pulse energies from 10 nJ to 60 nJ. The sample was annealed at 1000ºC for 3 hours in a N_2 atmosphere. Fig. 16(a),(b) shows optical, and confocal microscope images of the same area of the sample. The fluorescence rate and emission spectra from each static exposure spot was characterised using a confocal microscope at a range of optical excitation powers. Fig. 16(c) shows a zoomed in area around one of the brightest spots, written with a pulse energy of 40 nJ. The background corrected fluorescence rates were compared to that from a single NV center identified in the same sample, as shown in Fig. 16(d), in order to estimate the number of NV centers created by the femtosecond laser pulse. In this case, the femtosecond laser written spot is ~ 50 times brighter at saturation, suggesting the creation of about 50 NVs in the confocal focal volume of ~ 1 μm^3, and an NV density of ~ 5×10^{13} cm^{-3}.

Interestingly, a strong correlation between the femtosecond laser pulse energy and the estimated number of created NVs was not observed. Instead there was a stronger correlation between the brightness of the laser written spot, and the brightness of the unwritten area around it, which contains 'as grown' NVs. It can be seen in in Fig. 16(b) that the brighter laser written spots are situated in bands of higher numbers of 'as grown' NVs, corresponding to higher concentrations of substitutional nitrogen. This confirms that the number of femtosecond laser written NVs is strongly dependent on the available substitutional nitrogen in the lattice and motivates the investigation of diamond samples with yet higher nitrogen concentrations such as HPHT diamond (100 - 3000 ppm nitrogen).

5. Femtosecond laser writing of microfluidics on the surface of diamond

In the case of surface machining of diamond, the use of laser microfabrication technology has been usually limited to the investigation of the periodical sub-micron ripples observed on the sample surface after laser irradiation [115–121] and to the generation of channel-like microstructures with an average depth of less than half micron [122]. More recently, a collaboration between the groups of Eaton and Jedrkiewicz have shown the possibility to apply this technique combined with the use of ultrashort Bessel beams (BB) for a deep surface ablation of diamond in single pass [123,124], the resulting microstructures offering a great potential for microfluidics or biosensing applications.

Bessel beams are featured by a central core surrounded by rings which constitute the beam energy reservoir for a non-diffracting propagation. In the stationary nonlinear regime [125], a finite energy BB leaves in its wake, a uniform elongated plasma track, generated by the mean Bessel lobe, that is the main support for the nonlinear absorption of laser energy. Therefore, for a given fluence distributed in the focal volume, the ablation process by means of the Bessel beam turns out to be much more efficient with respect to the use of Gaussian beams, for which the Rayleigh range is at least one order of magnitude lower than the Bessel non-diffracting zone whose length depends on the beam cone angle θ.

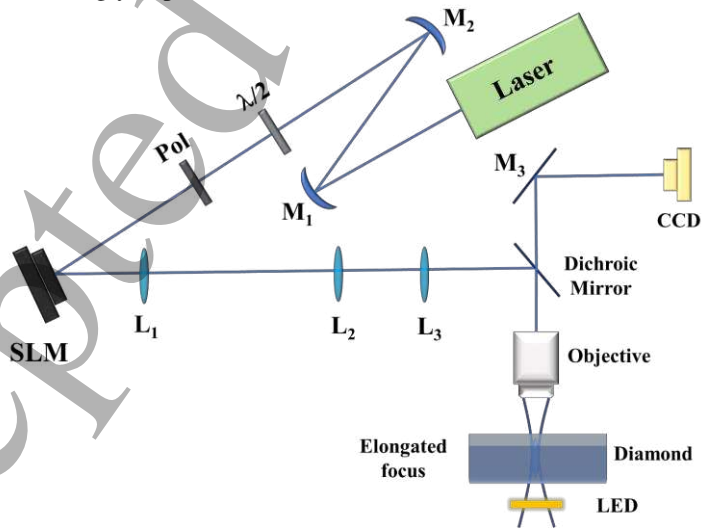

Fig. 17: Scheme of the experimental set-up of microfabrication. M_1 and M_2 are spherical mirrors used in a telescopic configuration to demagnify the laser beam; the lenses L_1, L_2 are used to image the BB generated by the SLM onto the micromachining set up, while L_3 coupled to the microscope objective demagnifies the BB at the sample position. All lenses have 30 cm focal length while the objective focal length is 9 mm [124].

Single pass tracks were first obtained as a function of different writing speeds [124], showing the possibility to tailor the cross-section of the obtained trenches that can be generated with arbitrary length at the diamond surface. It was observed that while the depth of the trenches is determined by the writing speed, their transverse width depends on the pulse energy. The pulse energy can be adjusted in such a way so that only the central lobe of the BB or the former together with a few surrounding rings affect the ablation process. In Fig. 18 one can see how the lateral rings of the BB affect the side of the written tracks, leaving on the surface, traces around the V-shaped 3D microstructures. In general, these tracks are featured by a deeper central trench created by the BB central core during the nonlinear absorption process. Scanning electron microscopy (SEM) images have highlighted the presence of nanogrooves inside the walls of the trenches, with orientation depending on the beam polarization. Homogeneous microchannels at the very depth of smooth and regular V-shaped trenches (such as those of Fig. 18(a) and (b)), were clearly revealed [123].

The laser micromachining technology combined with a beam shaping technique to generate ultrashort Bessel beams, has thus allowed to deeply ablate diamond surfaces in a single pass. The results have highlighted the possibility to tailor the surface features of the ablated structures on the micro-nano scale and thus to obtain channel-like microstructures potentially useful for microfluidics applications, with sensing functionality provided by NV centers.

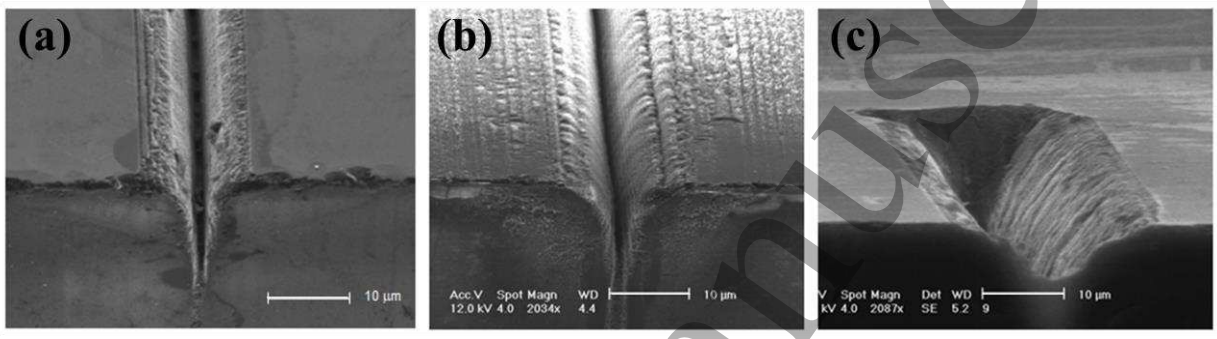

Fig. 18: Tilted view SEM images of microtracks machined in single pass on the diamond surface by means of a femtosecond pulsed Bessel beam with core size of about 0.7 µm (FHWM) in air, for different pulse energies. The scale bar for all SEM images is 10 µm. In (a), (b) and (c) the writing speed corresponded to having 280 spatially superimposed pulses. The energy per pulse was E = 3.5 µJ in (a), 7 µJ in (b) and 10 µJ in (c) [124].

6. Conclusions

In this Review, we demonstrated how the femtosecond laser writing technique can be applied to fabricate photonic and microfluidic networks in diamond, exhibiting exceptional performance. A novel laser writing procedure consisting of a single focused femtosecond laser pulse followed by a lower energy pulse train enables the formation of outstanding quality single NV centers with 100% yield. Furthermore, we have shown that laser writing of a high density of NVs is possible, boosting the sensitivity of quantum sensing. In addition, we have reported initial prototype devices which integrate laser-written NV centers, optical waveguides and microchannels, which could find use as quantum-based electric and magnetic field sensors.

The development of novel, biocompatible nanoscale, ultrasensitive imaging and sensing techniques is set to become one of the most important contributions of modern physics to society, with real potential impact for life sciences.

Laser written optical waveguides and NV centers could also be exploited in tomorrow's quantum computers. NVs interrogated by optical waveguides could enable a scalable diamond-based quantum computer based on long-range entanglement. Quantum information systems exploit the superposition and entanglement of qubits for a paradigm shift in the ability to perform tasks such as factoring large numbers or modelling nanoscale systems. Quantum computing is also ideally suited to solve macro-scale many-variable problems such as predicting the global climate and predict trends in the stock market.

Acknowledgements

The authors acknowledge support from FP7 DiamondFab CONCERT Japan project, DIAMANTE MIUR-SIR grant, FemtoDiamante Cariplo ERC reinforcement grant, University of Calgary's Eyes High Postdoctoral Fellowship program, NSERC Discovery Grant, NSERC Discovery Accelerator Supplement, NSERC Research Tools and Instruments, CFI. We thank Prof. Guglielmo Lanzani and Dr. Luigino Criante for the use of the FemtoFab facility at CNST - IIT Milano for the laser fabrication experiments.

References

[1] Aharonovich I, Greentree A D and Prawer S 2011 *Nat. Photonics* **5** 397–405

[2] Balasubramanian G, Neumann P, Twitchen D, Markham M, Kolesov R, Mizuochi N, Isoya J, Achard J, Beck J, Tissler J, Jacques V, Hemmer P R, Jelezko F and Wrachtrup J 2009 *Nat. Mater.* **8** 383–7

[3] Doherty M W, Dolde F, Fedder H, Jelezko F, Wrachtrup J, Manson N B and Hollenberg L C L 2012 *Phys. Rev. B* **85** 205203

[4] Dolde F, Fedder H, Doherty M W, Nöbauer T, Rempp F, Balasubramanian G, Wolf T, Reinhard F, Hollenberg L C L, Jelezko F and Wrachtrup J 2011 *Nat. Phys.* **7** 459–63

[5] Childress L, Walsworth R and Lukin M 2014 *Phys. Today* **67** 38–43

[6] Lenzini F, Gruhler N, Walter N and Pernice W H P 2018 *Adv. Quantum Technol.* 1800061

[7] Degen C 2008 *Nat. Nanotechnol.* **3** 643–4

[8] Barclay P E, Fu K-M C, Santori C, Faraon A and Beausoleil R G 2011 *Phys. Rev. X* **1** 011007

[9] Fu K-M C, Santori C, Barclay P E, Aharonovich I, Prawer S, Meyer N, Holm A M and Beausoleil R G 2008 *Appl. Phys. Lett.* **93** 234107

[10] Olivero P, Rubanov S, Reichart P, Gibson B C, Huntington S T, Rabeau J, Greentree A D, Salzman J, Moore D, Jamieson D N and Prawer S 2005 *Adv. Mater.* **17** 2427–30

[11] Faraon A, Santori C, Huang Z, Acosta V M and Beausoleil R G 2012 *Phys. Rev. Lett.* **109** 033604

[12] Hiscocks M P, Ganesan K, Gibson B C, Huntington S T, Ladouceur F and Prawer S 2008 *Opt. Express* **16** 19512

[13] Burek M J, Chu Y, Liddy M S Z, Patel P, Rochman J, Meesala S, Hong W, Quan Q, Lukin M D and Lončar M 2014 *Nat. Commun.* **5** 5718

[14] Atikian H A, Latawiec P, Burek M J, Sohn Y-I, Meesala S, Gravel N, Kouki A B and Lončar M 2017 *APL Photonics* **2** 051301

[15] Khanaliloo B, Jayakumar H, Hryciw A C, Lake D P, Kaviani H and Barclay P E 2015 *Phys. Rev. X* **5** 041051

[16] Khanaliloo B, Mitchell M, Hryciw A C and Barclay P E 2015 *Nano Lett.* **15** 5131–6

[17] Lagomarsino S, Olivero P, Bosia F, Vannoni M, Calusi S, Giuntini L and Massi M 2010 *Phys. Rev. Lett.* **105** 233903

[18] Jin H, Turaga S P, Vanga S K and Bettiol A A 2018 *Opt. Lett.* **43** 2648

[19] Bernardi E, Nelz R, Sonusen S, Neu E, Bernardi E, Nelz R, Sonusen S and Neu E 2017 *Crystals* **7** 124

[20] Davis K M, Miura K, Sugimoto N and Hirao K 1996 *Opt. Lett.* **21** 1729

[21] Du D, Liu X, Korn G, Squier J and Mourou G 1994 *Appl. Phys. Lett.* **64** 3071–3

[22] Stuart B C, Feit M D, Rubenchik A M, Shore B W and Perry M D 1995 *Phys. Rev. Lett.* **74** 2248–51

[23] Schaffer C B, Brodeur A and Mazur E 2001 *Meas. Sci. Technol.* **12** 1784–94

[24] Glezer E N, Milosavljevic M, Huang L, Finlay R J, Her T-H, Callan J P and Mazur E 1996 *Opt. Lett.* **21** 2023

[25] Streltsov A M and Borrelli N F 2002 *J. Opt. Soc. Am. B* **19** 2496

[26] Schaffer C B, García J F and Mazur E 2003 *Appl. Phys. A Mater. Sci. Process.* **76** 351–4

[27] Eaton S M, Zhang H, Herman P R, Yoshino F, Shah L, Bovatsek J and Arai A Y 2005 *Opt. Express* **13** 4708

[28] Chan J W, Huser T, Risbud S and Krol D M 2001 *Opt. Lett.* **26** 1726

[29] Fernandez T T, Sakakura M, Eaton S M, Sotillo B, Siegel J, Solis J, Shimotsuma Y and Miura K 2018 *Prog. Mater. Sci.* **94** 68–113

[30] Fernandez T T, Hernandez M, Sotillo B, Eaton S M, Jose G, Osellame R, Jha A, Fernandez P and Solis J 2014 *Opt. Express* **22** 15298

[31] Shimizu M, Sakakura M, Kanehira S, Nishi M, Shimotsuma Y, Hirao K and Miura K 2011 *Opt. Lett.* **36** 2161

[32] Della Valle G, Osellame R and Laporta P 2009 *J. Opt. A Pure Appl. Opt.* **11** 013001

[33] Gattass R R and Mazur E 2008 *Nat. Photonics* **2** 219–25

[34] Osellame R, Cerullo G and Ramponi R 2012 *Springer Sci. Bus. Media* **123**

[35] Chen F and de Aldana J R V 2014 *Laser Photon. Rev.* **8** 251–75

[36] Gorelik T, Will M, Nolte S, Tuennermann A and Glatzel U 2003 *Appl. Phys. A Mater. Sci. Process.* **76** 309–11

[37] Apostolopoulos V, Laversenne L, Colomb T, Depeursinge C, Salathé R P, Pollnau M, Osellame R, Cerullo G and Laporta P 2004 *Appl. Phys. Lett.* **85** 1122–4

[38] Burghoff J, Nolte S and Tünnermann A 2007 *Appl. Phys. A* **89** 127–32

[39] Nejadmalayeri A H, Herman P R, Burghoff J, Will M, Nolte S and Tünnermann A 2005 *Opt. Lett.* **30** 964

[40] Eaton S M, Merchant C A, Iyer R, Zilkie A J, Helmy A S, Aitchison J S, Herman P R, Kraemer D, Miller R J D, Hnatovsky C and Taylor R S 2008 *Appl. Phys. Lett.* **92** 081105

[41] Calmano T, Ams M, Dekker P, Withford M J and Kränkel C 2017 *Opt. Mater. Express* **7** 2777

[42] Macdonald J R, Thomson R R, Beecher S J, Psaila N D, Bookey H T and Kar A K 2010 *Opt. Lett.* **35** 4036

[43] Laurell F, Calmano T, Müller S, Zeil P, Canalias C and Huber G 2012 *Opt. Express* **20** 22308

[44] Corrielli G, Seri A, Mazzera M, Osellame R and de Riedmatten H 2016 *Phys. Rev. Appl.* **5** 054013

[45] Taccheo S, Della Valle G, Osellame R, Cerullo G, Chiodo N, Laporta P, Svelto O, Killi A, Morgner U, Lederer M and Kopf D 2004 *Opt. Lett.* **29** 2626

[46] Eaton S M, Zhang H, Ng M L, Li J, Chen W-J, Ho S and Herman P R 2008 *Opt. Express* **16** 9443

[47] Vázquez M R, Sotillo B, Rampini S, Bharadwaj V, Gholipour B, Fernández P, Ramponi R, Soci C and Eaton S M 2018 *J. Phys. Photonics* **1** 015006

[48] Arriola A, Gross S, Ams M, Gretzinger T, Le Coq D, Wang R P, Ebendorff-Heidepriem H, Sanghera J, Bayya S, Shaw L B, Ireland M, Tuthill P and Withford M J 2017 *Opt. Mater. Express* **7** 698

[49] Torchia G A, Rodenas A, Benayas A, Cantelar E, Roso L and Jaque D 2008 *Appl. Phys. Lett.* **92** 111103

[50] Eaton S M, De Marco C, Martinez-Vazquez R, Ramponi R, Turri S, Cerullo G and Osellame R 2012 *J. Biophotonics* **5** 687–702

[51] Hnatovsky C, Taylor R S, Simova E, Rajeev P P, Rayner D M, Bhardwaj V R and Corkum P B 2006 *Appl. Phys. A* **84** 47–61

[52] Suriano R, Kuznetsov A, Eaton S M, Kiyan R, Cerullo G, Osellame R, Chichkov B N, Levi M and Turri S 2011 *Appl. Surf. Sci.* **257** 6243–50

[53] Farsari M and Chichkov B N 2009 *Nat. Photonics* **3** 450–2

[54] Raimondi M, Nava M, Eaton S, Bernasconi A, Vishnubhatla K, Cerullo G, Osellame R, Raimondi M T, Nava M M, Eaton S M, Bernasconi A, Vishnubhatla K C, Cerullo G and Osellame R 2014 *Micromachines* **5** 341–58

[55] Serra F, Eaton S M, Cerbino R, Buscaglia M, Cerullo G, Osellame R and Bellini T 2013 *Adv. Funct. Mater.* **23** 4060–4060

[56] De Marco C, Gaidukeviciute A, Kiyan R, Eaton S M, Levi M, Osellame R, Chichkov B N and Turri S 2013 *Langmuir* **29** 426–31

[57] Streltsov A M and Borrelli N F 2001 *Opt. Lett.* **26** 42

[58] Homoelle D, Wielandy S, Gaeta A L, Borrelli N F and Smith C 1999 *Opt. Lett.* **24** 1311

[59] Fernandes L A, Grenier J R, Herman P R, Aitchison J S and Marques P V S 2011 *Opt. Express* **19** 18294

[60] Lai Y, Martinez A, Khrushchev I and Bennion I 2006 *Opt. Lett.* **31** 1672

[61] Minoshima K, Kowalevicz A, Ippen E and Fujimoto J 2002 *Opt. Express* **10** 645

[62] Fernandez T T, Eaton S M, Della Valle G, Vazquez R M, Irannejad M, Jose G, Jha A, Cerullo G, Osellame R and Laporta P 2010 *Opt. Express* **18** 20289

[63] Thomson R R, Kar A K and Allington-Smith J 2009 *Opt. Express* **17** 1963

[64] Meany T, Gräfe M, Heilmann R, Perez-Leija A, Gross S, Steel M J, Withford M J and Szameit A 2015 *Laser Photon. Rev.* **9** 363–84

[65] Zhang H, Aitchison J, Stewart, Li J, Ng M, Li, Herman P R, Iyer R, Eaton S M, Ho S and Chen W-J 2009 *J. Light. Technol.* **27** 1079–85

[66] Zhang H, Ho S, Eaton S M, Li J and Herman P R 2008 *Opt. Express* **16** 14015
[67] Sugioka K, Cheng Y and Midorikawa K 2005 *Appl. Phys. A* **81** 1–10
[68] Haque M, Lee K K C, Ho S, Fernandes L A and Herman P R 2014 *Lab Chip* **14** 3817–29
[69] Markham M L, Dodson J M, Scarsbrook G A, Twitchen D J, Balasubramanian G, Jelezko F and Wrachtrup J 2011 *Diam. Relat. Mater.* **20** 134–9
[70] Harris D C 1994 *SPIE Proceedings* vol 2286 pp 218–28
[71] Burghoff J, Grebing C, Nolte S and Tünnermann A 2006 *Appl. Phys. Lett.* **89** 081108
[72] Prawer S, Jamieson D N and Kalish R 1992 *Phys. Rev. Lett.* **69** 2991–4
[73] Kononenko V V, Pimenov S M, Kononenko T V, Konov V I, Fischer P, Romano V, Weber H P, Khomich A V and Khmelnitskiy R A 2003 *Diam. Relat. Mater.* **12** 277–82
[74] Shimotsuma Y, Sakakura M, Kanehira S, Qiu J, Kazansky P G, Miura K, Fujita K and Hirao K 2006 *JLMN-Journal of Laser Micro/Nanoengineering* **1**
[75] Neff M, Kononenko T V., Pimenov S M, Romano V, Lüthy W and Konov V I 2009 *Appl. Phys. A* **97** 543–7
[76] Sun B, Salter P S and Booth M J 2014 *Appl. Phys. Lett.* **105** 231105
[77] Kononenko T V, Meier M, Komlenok M S, Pimenov S M, Romano V, Pashinin V P and Konov V I 2008 *Appl. Phys. A* **90** 645–51
[78] Simmonds R D, Salter P S, Jesacher A and Booth M J 2011 *Opt. Express* **19** 24122
[79] Kumar S, Sotillo B, Chiappini A, Ramponi R, Di Trapani P, Eaton S M and Jedrkiewicz O 2017 *Appl. Phys. A* **123** 698
[80] Booth M J, Forcolin G T, Grilj V, Hamilton B, Haughton I, McGowan M, Murphy S A, Oh A, Salter P S, Sudić I and Skukan N 2017 *Diam. Relat. Mater.* **77** 137–45
[81] Murphy S A, Booth M, Li L, Oh A, Salter P, Sun B, Whitehead D and Zadoroshnyj A 2017 *Nucl. Instruments Methods Phys. Res. Sect. A Accel. Spectrometers, Detect. Assoc. Equip.* **845** 136–8
[82] Khomich A A, Ashikkalieva K K, Bolshakov A P, Kononenko T V., Ralchenko V G, Konov V I, Oliva P, Conte G and Salvatori S 2018 *Diam. Relat. Mater.* **90** 84–92
[83] Sun B, Salter P S and Booth M J 2016 *SPIE Proceedings* vol 9736 p 973612
[84] Sotillo B, Bharadwaj V, Hadden J, Rampini S, Chiappini A, Fernandez T, Armellini C, Serpengüzel A, Ferrari M, Barclay P, Ramponi R, Eaton S, Sotillo B, Bharadwaj V, Hadden J P, Rampini S, Chiappini A, Fernandez T T, Armellini C, Serpengüzel A, Ferrari M, Barclay P E, Ramponi R and Eaton S M 2017 *Micromachines* **8** 60
[85] Sotillo B, Bharadwaj V, Hadden J P, Sakakura M, Chiappini A, Fernandez T T, Longhi S, Jedrkiewicz O, Shimotsuma Y, Criante L, Osellame R, Galzerano G, Ferrari M, Miura K, Ramponi R, Barclay P E and Eaton S M 2016 *Sci. Rep.* **6** 35566
[86] Schwan J, Ulrich S, Batori V, Ehrhardt H and Silva S R P 1998 *J. Appl. Phys.* **80** 440
[87] Salter P S, Booth M J, Courvoisier A, Moran D A J and MacLaren D A 2017 *Appl. Phys. Lett.* **111** 081103
[88] Sotillo B, Chiappini A, Bharadwaj V, Hadden J P, Bosia F, Olivero P, Ferrari M, Ramponi R, Barclay P E and Eaton S M 2018 *Appl. Phys. Lett.* **112** 031109
[89] Courvoisier A, Booth M J and Salter P S 2016 *Appl. Phys. Lett.* **109** 031109
[90] Bharadwaj V, Wang Y, Fernandez T T, Ramponi R, Eaton S M and Galzerano G 2018 *Opt. Mater.* **85** 183–5
[91] Hensen B, Bernien H, Dréau A E, Reiserer A, Kalb N, Blok M S, Ruitenberg J, Vermeulen R F L, Schouten R N, Abellán C, Amaya W, Pruneri V, Mitchell M W, Markham M, Twitchen D J, Elkouss D, Wehner S, Taminiau T H and Hanson R 2015 *Nature* **526** 682–6
[92] Taylor J M, Cappellaro P, Childress L, Jiang L, Budker D, Hemmer P R, Yacoby A, Walsworth R and Lukin M D 2008 *Nat. Phys.* **4** 810–6
[93] Latawiec P, Venkataraman V, Shams-Ansari A, Markham M and Lončar M 2018 *Opt. Lett.* **43** 318
[94] Bharadwaj V, Courvoisier A, Fernandez T T, Ramponi R, Galzerano G, Nunn J, Booth M J, Osellame R, Eaton S M and Salter P S 2017 *Opt. Lett.* **42** 3451
[95] Rabeau J R, Reichart P, Tamanyan G, Jamieson D N, Prawer S, Jelezko F, Gaebel T, Popa I, Domhan M and Wrachtrup J 2006 *Appl. Phys. Lett.* **88** 023113
[96] Orwa J O, Santori C, Fu K M C, Gibson B, Simpson D, Aharonovich I, Stacey A, Cimmino A, Balog P, Markham M, Twitchen D, Greentree A D, Beausoleil R G and Prawer S 2011 *J. Appl. Phys.* **109** 083530
[97] Pezzagna S, Naydenov B, Jelezko F, Wrachtrup J and Meijer J 2010 *New J. Phys.* **12** 065017
[98] Chen Y-C, Salter P S, Knauer S, Weng L, Frangeskou A C, Stephen C J, Ishmael S N, Dolan P R, Johnson S, Green B L, Morley G W, Newton M E, Rarity J G, Booth M J and Smith J M 2017 *Nat. Photonics* **11** 77–80
[99] Naydenov B, Reinhard F, Lämmle A, Richter V, Kalish R, D'Haenens-Johansson U F S, Newton M, Jelezko F and Wrachtrup J 2010 *Appl. Phys. Lett.* **97** 242511
[100] Rondin L, Tetienne J-P, Hingant T, Roch J-F, Maletinsky P and Jacques V 2014 *Reports Prog. Phys.* **77** 056503
[101] Stephen C J, Green B L, Lekhai Y N D, Weng L, Hill P, Johnson S, Frangeskou A C, Diggle P L, Strain M J, Gu E, Newton M E, Smith J M, Salter P S and Morley G W 2018 *arXiv:1807.03643*
[102] Hong S, Grinolds M S, Pham L M, Le Sage D, Luan L, Walsworth R L and Yacoby A 2013 *MRS Bull.* **38** 155–61
[103] Chen E H, Clevenson H A, Johnson K A, Pham L M, Englund D R, Hemmer P R and Braje D A 2017 *Phys. Rev. A* **95** 053417
[104] Hadden J P, Bharadwaj V, Sotillo B, Rampini S, Osellame R, Witmer J, Jayakumar H, Fernandez T T, Chiappini A, Armellini C, Ferrari M, Ramponi R, Barclay P E and Eaton S M 2017 *arXiv:1701.05885 (Supplementary)*
[105] Chen Y-C, Griffiths B, Weng L, Nicley S, Ishmael S N, Lekhai Y, Johnson S, Stephen C J, Green B L, Morley G W, Newton M E, Booth M J, Salter P S and Smith J M 2018 *arXiv:1807.04028*
[106] Benayas A, Silva W F, Jacinto C, Cantelar E, Lamela J, Jaque F, Vázquez de Aldana J R, Torchia G A, Roso L, Kaminskii A A and Jaque D 2010 *Opt. Lett.* **35** 330
[107] Martínez de Mendívil J, Sola D, Vázquez de Aldana J R, Lifante G, de Aza A H, Pena P and Peña J I 2015 *J. Appl. Phys.* **117** 043104
[108] Ferrari A C and Robertson J 2000 *Phys. Rev. B* **61** 14095–107
[109] Kalish R, Reznik A, Prawer S, Saada D and Adler J 1999 *Phys. status solidi* **174** 83–99
[110] Dolde F, Jakobi I, Naydenov B, Zhao N, Pezzagna S, Trautmann C, Meijer J, Neumann P, Jelezko F and Wrachtrup J 2013 *Nat. Phys.* **9** 139–43
[111] Hadden J P, Bharadwaj V, Sotillo B, Rampini S, Osellame R, Witmer J D, Jayakumar H, Fernandez T T, Chiappini A, Armellini C, Ferrari M, Ramponi R, Barclay P E and Eaton S M 2018 *Opt. Lett.* **43** 3586
[112] Balasubramanian G, Chan I Y, Kolesov R, Al-Hmoud M, Tisler J, Shin C, Kim C, Wojcik A, Hemmer P R, Krueger A, Hanke T, Leitenstorfer A, Bratschitsch R, Jelezko F and Wrachtrup J 2008 *Nature* **455** 648–51
[113] Clevenson H, Trusheim M E, Teale C, Schröder T, Braje D and Englund D 2015 *Nat. Phys.* **11** 393–7
[114] Barry J F, Turner M J, Schloss J M, Glenn D R, Song Y, Lukin M D, Park H and Walsworth R L 2016 *Proc. Natl. Acad. Sci. U. S. A.* **113** 14133–8
[115] Ozkan A M, Malshe A P, Railkar T A, Brown W D, Shirk M D and Molian P A 1999 *Appl. Phys. Lett.* **75** 3716
[116] Wu Q, Ma Y, Fang R, Liao Y, Yu Q, Chen X and Wang K 2003 *Appl. Phys. Lett.* **82** 1703–5
[117] Shinoda M, Gattass R R and Mazur E 2009 *J. Appl. Phys.* **105** 053102
[118] Kumar Kuntumalla M, Rajamudili K, Rao Desai N and Srikanth V V S S 2014 *Appl. Phys. Lett.* **104** 161607
[119] Trucchi D, Bellucci A, Girolami M, Mastellone M, Orlando S, Trucchi D M, Bellucci A, Girolami M, Mastellone M and Orlando S 2017 *Coatings* **7** 185

[120] Granados E, Martinez-Calderon M, Gomez M, Rodriguez A and Olaizola S M 2017 *Opt. Express* **25** 15330
[121] Abdelmalek A, Sotillo B, Bedrane Z, Bharadwaj V, Pietralunga S, Ramponi R, Amara E-H and Eaton S M 2017 *AIP Adv.* **7** 105105
[122] Su S, Li J, Lee G C B, Sugden K, Webb D and Ye H 2013 *Appl. Phys. Lett.* **102** 231913
[123] Kumar S, Eaton S M, Bollani M, Sotillo B, Chiappini A, Ferrari M, Ramponi R, Di Trapani P and Jedrkiewicz O 2018 *Sci. Rep.* **8** 14021
[124] Jedrkiewicz O, Kumar S, Sotillo B, Bollani M, Chiappini A, Ferrari M, Ramponi R, Di Trapani P and Eaton S M 2017 *Opt. Mater. Express* **7** 1962
[125] Porras M A, Parola A, Faccio D, Dubietis A and Trapani P Di 2004 *Phys. Rev. Lett.* **93** 153902